ALEPH 93-24
PHYSIC 93-16
D.Abbaneo et al.
11 February 1993

Measurement of the $Z \to b\bar{b}$ forward − backward asymmetry and of the χ mixing parameter from high $p_\perp$ leptons

D. Abbaneo, C. Bozzi, F. Ligabue, R. Tenchini and A. Venturi

Abstract

The $Z \to b\bar{b}$ forward–backward asymmetry and the χ mixing parameter have been measured starting form a sample of about 430,000 hadronic Z decays collected in 1990 and 1991. $Z \to b\bar{b}$ events have been tagged through the detection of high–$p_\perp$ leptons (electrons or muons) in the event. The forward–backward asymmetry is determined by fitting the $\cos\theta$ angular distribution of the candidate $b\bar{b}$ events. After correcting for wash–out effects like $B^0\bar{B}^0$ mixing, we get, for events at the Z peak, $A_{FB}(b) = (7.9 \pm 1.6 \pm 0.8)\%$. The mixing parameter has been measured by counting the number of same sign and opposite sign dileptons an correcting for non–primary b contamination. We get $\chi = (11.2 \pm 1.5 \pm 0.8)\%$.

Contents

1 Introduction

We have measured the $b\bar{b}$ forward backward asymmetry and the χ mixing parameter from about 430 000 hadronic events collected in 1990 and 1991. The $b\bar{b}$ asymmetry is determined from high $p_\perp$ leptons as described in paper [1] and previous notes [2, 3]. The raw asymmetry of a high b purity $q\bar{q}$ sample is found by fitting the $\cos\theta$ angular distribution with a likelihood function. The $b\bar{b}$ asymmetry is then extracted taking into account effects which wash out the asymmetry (like, for instance, $b\bar{b}$ mixing) and background contamination. The high $p_\perp$ dilepton sample has been used to measure the mixing parameter by counting the number of same sign and opposite sign dileptons an correcting for non–primary b contamination. This note contains a detailed description of the two analysis (sections 3 and 4). Since lepton tagging is a fundamental tool for both, there is a rather long discussion on muon identification, including an Appendix on muon background, which has been source of joy and pain for some of us. Electron identification is just mentioned and is fully described in other notes [19, 3].

2 Selection of a High Purity b Sample

The set of cuts described below leads to the selection of a sample of hadronic events, in which one of the jets contains a high p and $p_\perp$ candidate electron or muon. This sample includes events from various kind of processes, both from actual b semileptonic decays and from 'background' processes. The cuts are optimized in order to achieve the best possible fraction of events where the lepton comes from a direct semileptonic decay of a beauty hadron $B \to l\bar{\nu}X$ (which we call a *primary* b). We call such fraction the *purity* of our sample.

In the following the details of the event selection are described. The first step is a general selection of hadronic events among the data recorded by ALEPH.

2.1 Hadronic event selection

Hadronic events are selected using charged track information alone: at least 5 tracks must be reconstructed by the TPC in the event; they must be "good" tracks according to the following definition:

- the track must form an angle greater than 18.2° with the beam axis: this ensures that at least 6 pad rows in the TPC are traversed

- the number of TPC three–dimensional points used in the fit for the track helix must be at least 4. This eliminates most unphysical fake tracks and badly fitted ones

- the track must pass through a cylinder centred around the fitted average beam position, with a radius of 2 cm and a length of 10 cm. This cut rejects badly fitted tracks or particles originating from a vertex different from the interaction point, as well as cosmic background.

Moreover, a cut on the total visible energy is applied in order to remove $\gamma\gamma$ events and beam–gas interactions: the sum of momenta of all the reconstructed charged tracks must be greater than 10% of the centre-of-mass energy. The total efficiency of this selection is 94.8% [8] and is independent of flavour whithin 1%; according to Monte Carlo predictions, the background contaminations from two–photon events and $Z \to \tau^+\tau^-$ are less than 0.3%. The precise knowledge of the absolute efficiency of this selection method is not relevant for our purposes, since we are not dealing with absolute measurements. However, a poor knowledge of the relative efficiency among various flavours would reflect into a bad evaluation of the flavour composition of our final selected sample, which would turn into a systematic error on final values. We have no indication so far that this might be the case, and in any case a variation of a few percent of this relative efficiency in the case of b would lead to a negligible contribution to the systematic error as compared to other sources.

We have analysed data collected by ALEPH in 1990 and 1991. We decided to discard 1989 data because the negligible improvement in statistics could not justify the special effort of dealing with data where the apparatus was not at its best performance level. For instance, muon identification was not available in the endcaps, and so only electrons could have been used for 1989 data.

Our data sample consists of 434 064 $Z^0 \to q\bar{q}$ events, about one third of which were recorded in 1990.

We have restricted our analysis to the runs which fulfil the Heavy Flavours group data quality requirements, where the whole detector was in a reasonable shape for both muon and electron identification.

2.2 Muon Identification

Muons are identified in ALEPH making use of the tracking capabilities of the Hadron Calorimeter, together with the Muon Chamber information. Basically, muon identification in HCAL consists in extrapolating a TPC track through the calorimeter, and counting how many HCAL digital hits fall in the neighbourhood of the extrapolated track. This allows the discrimination of particles which penetrate through the whole depth of the calorimeter.

Each track with momenta greater than 1.5 GeV/c is extrapolated (as if it were a muon) through the HCAL material taking into account a detailed magnetic field map and estimated energy losses. A "road" is opened around the extrapolated track, whose width is 3 times the standard deviation on the estimated extrapolation error due to multiple scattering[1]. An HCAL plane is said to be *expected* to fire if the extrapolated tracks intersects it within an active region; the plane is said to have *fired* if a digital hit lies within the multiple scattering road; the number of adjacent firing tubes the hit is made of must not be greater than 3 [4].

HCAL plane efficiency Originally, plane inefficiencies in the Monte Carlo are only ascribed to the geometrical acceptance of a tube (which causes a 10% inefficiency due to plastic walls) and to dead regions between tubes such as spacers or iron walls. The true plane inefficiency is actually higher than that, mainly because the effect of the hardware threshold, which is necessary in order to suppress noise, is not fully simulated in Monte Carlo. A further, less important, source of hardware ineffeciency is due to dead tubes and faults in the digital readout electronics. The plane efficiency is mapped in a detailed way in the Monte Carlo using $Z \rightarrow \mu^+\mu^-$ events in data. Clearly, for this purpose the sample of $Z \rightarrow \mu^+\mu^-$ events has to be selected through an algorithm which doesn't make use of the HCAL information.

A very pure sample of $Z \rightarrow \mu^+\mu^-$ events is selected by taking events with two good tracks, which must be back-to-back (*i.e.* they must lie one in each thrust hemisphere); one of the two tracks must carry more than 80%, and the other more than 50% of the beam energy; moreover the total energy measured by the wires in the Electromagnetic Calorimeter must not exceed 10% of the centre-of-mass energy. The Monte Carlo predicts for such

[1] An offset of 3 *cm* is added to the "road" width to take into account possible misalignment of the tubes inside HCAL

a selection a sample purity of over 99%, where most of the contaminating events are $\tau^+\tau^-$ events where both tau's have decayed to a muon (which, for our purposes, are exactly as useful as $Z \to \mu^+\mu^-$ events).

Such events are used to evaluate the efficiency of HCAL double planes, for each of the 24 modules (6 in each endcap and 12 supermodules in the barrel[2]). The efficiency is computed by counting how many times a plane that is crossed by an extrapolated track actually fires. The statistical precision which has been obtained on the average plane efficiency is of about 1% for the barrel and 2% for the endcaps. This definition includes the effect of plastic walls, spacers and other dead zones, which means that perfectly efficient tubes would not yield a 100% efficiency. In the Monte Carlo, tubes are described as having an efficiency of 87%, due to the effect of plastic walls. Adding other dead spaces yields an average global efficiency of 80%.

Shown in fig. 1 are the plane efficiencies, for 1991, 1990 and Monte Carlo data. Efficiencies in data are lower than in Monte Carlo: it turns out that real planes show a global 93% efficiency for firing in addition to the 80% overall geometrical efficiency present in the Monte Carlo and the endcaps are systematically lower than the barrel because of the different (and unfavourable) digital readout configuration. This information from real data is used to implement plane efficiencies inside the reconstruction code. The procedure consists in a random deletion of simulated hits in Monte Carlo events, the deletion in a certain plane occurring with a probability equal to the measured inefficiency. In this way we make sure that the observed behaviour of the detector in real data is correctly reproduced [5].

HCAL selection Muons are identified with cuts consistent with a track which penetrates through the whole depth of HCAL without showering. It is a nice feature of muons that such cuts can be independent of momentum, since a muon above 3 GeV/c penetrates up to the Muon Chambers: in addition, test-beam data show that — as we expect — there are no differences in the tube firing efficiency for muons from 5 to 50 GeV/c.

The cuts used to define a penetrating track are

- $N_{fir}/N_{exp} \geq 0.4$

[2]In the most recent Monte Carlo productions the efficiencies are evaluated for each of the 24 modules of the barrel

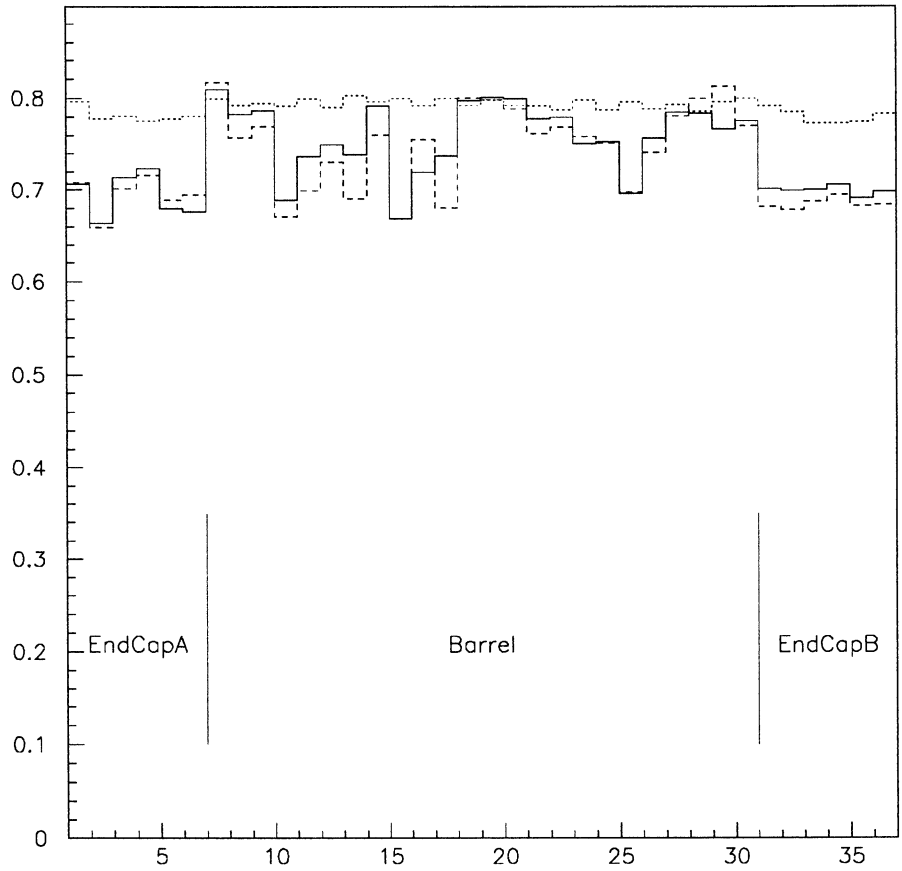

Figure 1: Average HCAL plane firing efficiencies for endcaps and barrel modules in 1991 (solid line), 1990 (dashed line) and Monte Carlo (dotted line).

- $N_{exp} \geq 10$
- $N_{10} > 4$

where N_{exp}, N_{fir} and N_{10} are, respectively, the number of expected planes, the number of actually firing planes, and the number of firing planes within the last ten expected associated to the track.

These cuts are suitable for isolated muons like $Z \rightarrow \mu^+\mu^-$ events or $\tau\tau$ events. On the other hand, for muon identification in the study of Z^0 decays into Heavy Flavour final states, some extra requirements are added to this standard ALEPH identification algorithm because in this case muons are hidden inside jets, which requires a better rejection power against hadron background.

Hit Multiplicity The digital pattern created by a hadron shower in the HCAL looks quite different from that created by a muon. This is easily seen "by eye", if one looks at the graphical event display both in Z^0 events (Monte Carlo and data) and in test–beam data.

This feature allows to develop rough but fast methods which are of great help in rejecting hadron showers. The one used in the ALEPH standard muon identification algorithm is based on a variable called X_{mult}. This variable is computed by counting all the HCAL digital hits within a cone of "radius" from 20 cm to 30 cm around the extrapolated track in the last eleven planes and dividing by the number of firing planes; in this way X_{mult} represents the average hit multiplicity per fired plane, which gives a measure on the lateral size of the digital pattern linked to the track.

The cut applied for muon identification is

$$X_{mult} \leq 1.5$$

which removes about 1% of the prompt muons in the Monte Carlo.

In fig. 2 the distributions for N_{fir}/N_{exp}, N_{10} and X_{mult} are shown for muons coming from $Z \rightarrow \mu^+\mu^-$ events and from pions produced in τ decays[3] (both from 1991 data).

[3]See the Appendix for the pions selection algorithm

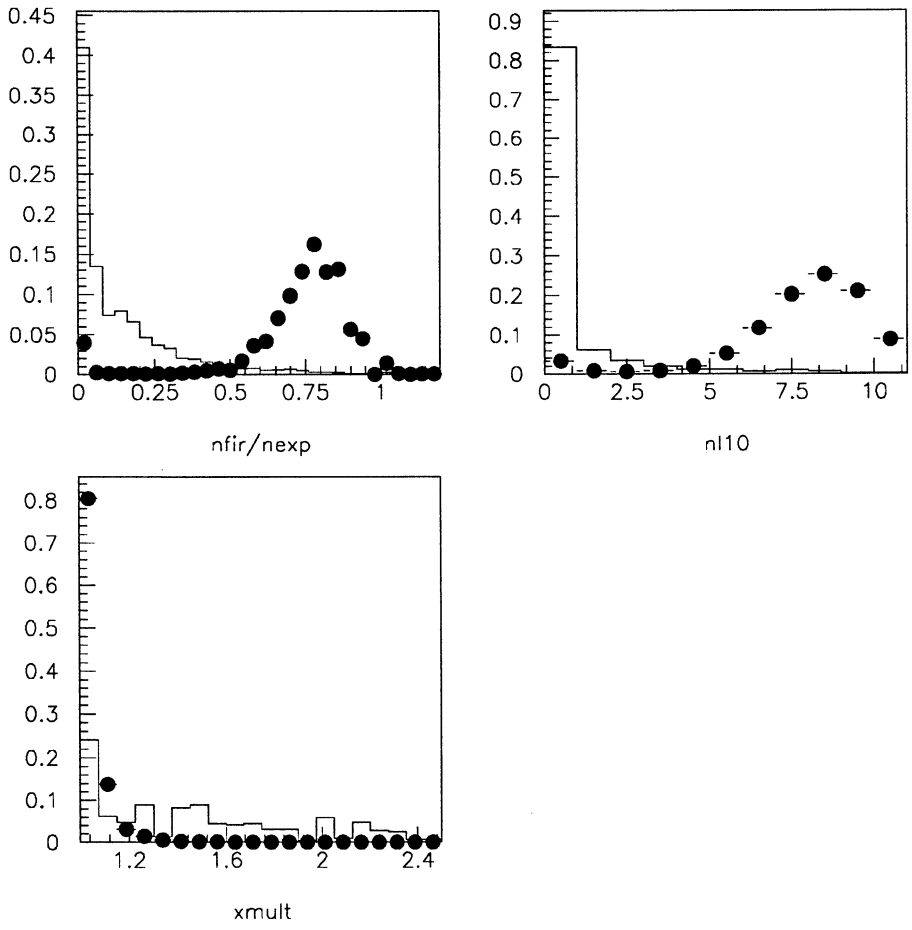

Figure 2: Distribution of N_{fir}/N_{exp}, N_{10} and X_{mult} for muons (dots) and pions (solid line).

Muon Chamber association The installation of the full Muon Detector, composed of two layers of chambers, was completed between the 1990 and 1991 running periods. During 1990 data–taking only the first layer of Muon Chambers was operational.

In a single layer of chambers a charged particle traversing the Hadron Calorimeter can generate up to two three–dimensional hits[4] in the Muon Detector, one for each tube plane inside a chamber (actually this is not strictly true, since there exist small angular regions of overlap where a track can traverse two chambers, both belonging to the first layer).

A track is defined to have hit the Muon Chambers if at least one of the two tube planes has yielded a two–dimensional hit (*i.e.* a cluster has been recostructed from both the X and the Y strips of the same plane) whose distance from the extrapolated track is less than 4 times the estimated multiple scattering standard deviation[5] [4].

The efficiency of the Muon Chambers has been measured with a procedure similar to what was used for the HCAL double planes, and again the results are inserted in the reconstruction program to account for the measured efficiencies through random hit deletion in Monte Carlo events. The efficiencies of the Muon Chambers for 1991 data are shown in fig. 3.

We found that the request of Muon Chamber association as a further cut for muon identification is very powerful for background rejection: from Monte Carlo it turns out that while about 85% of the muons which have been identified in HCAL are associated to a firing Muon Chamber, in the case of misidentified hadrons such a fraction reduces to 20%.

The reason for this is mainly twofold: first, requiring a hit in the Muon Chambers ensures that the particle has actually traversed the whole depth of the calorimeter, which may not always be the case for a track identified by the above HCAL cuts, as explained above; secondly, the Muon Chamber association requires a *two dimensional* matching between the track and a hit in the detector: this condition is less likely to be satisfied when the hit is due to a secondary particle produced inside a hadronic shower and leaking out of the calorimeter. Moreover, we recall that between the last active plane of the calorimeter and the Muon Chambers there is an additional 10 cm thick

[4]Hits on each muon chamber are actually two–dimensional, but the third coordinate is given by the known position of the chamber itself

[5]The hit is associated in any case if the distance is less then 5 *cm*

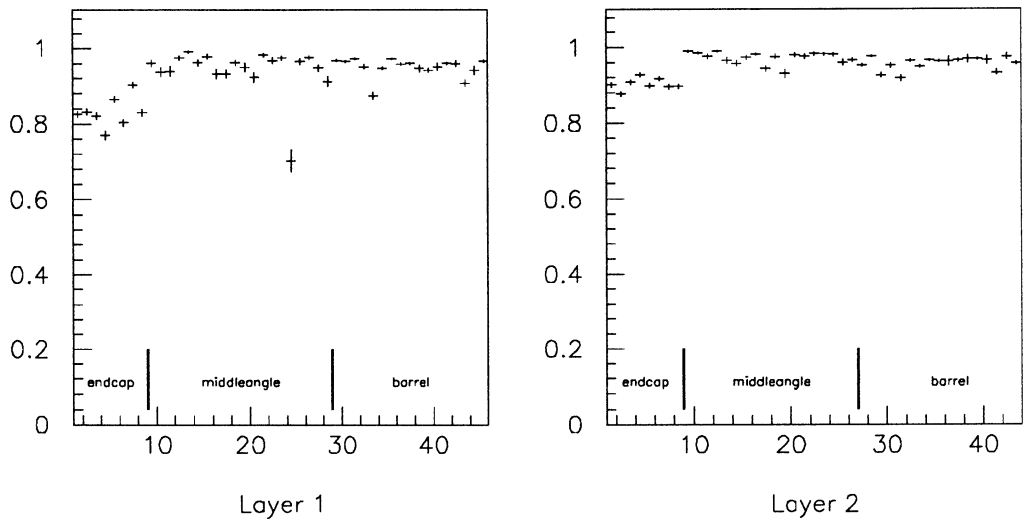

Figure 3: Efficiencies of the two Muon Chamber layers in 1991 (OR of the two planes of tubes).

iron slab, which acts as an additional muon filter.

These considerations make it easy to predict the effect of requiring a fired Muon Chamber: by reducing the hadron contamination inside the lepton sample, this will increase the primary b purity and correspondingly decrease the background from misidentified hadrons. The other sample components will stay to first approximation the same, since they don't depend on the performance of muon identification.

For the 1991 data, in order to be consistent with the 1990 analysis, we kept the requirement of at least one associated hit in the Muon Chambers, either in the first or in the second layer. The addition of the outer layer then simply causes an increase in the muon detection efficiency.

Shadowing Due to the high track multiplicity inside a jet, and due to the fact that the HCAL tracking is only in one projection, the multiple scattering "roads" opened around different tracks can overlap, and the same hit can be associated to more than one track. When two tracks happen to have common hits, they are said to be *shadowing* each other. The shadowing ambiguity becomes annoying when two shadowing tracks get both identified as muons

	$p_\perp < 1.25$ GeV/c	$p_\perp > 1.25$ GeV/c
prompt muons (%)	23 ± 1	20 ± 1
hadrons (%)	50 ± 3	28 ± 7

Table 1: Fraction of *shadowed* prompt muons and fakes.

	$p_\perp < 1.25$ GeV/c	$p_\perp > 1.25$ GeV/c
prompt muons (%)	0.4 ± 0.2	< 0.1
hadrons (%)	22 ± 2	15 ± 5

Table 2: Fraction of prompt muons and fakes rejected by the shadowing algorithm.

and one has to perform a choice between the two candidates. The best handle to solve the ambiguity comes from the Muon Chambers which, providing three dimensional hits, in most cases leave no room for doubt as to which of the two tracks is the true muon. In case *both* tracks share exactly the same Muon Chamber hits, the one with the minimum hit-to-track distance is chosen[6]. In table 1 the fraction of identified prompt muons and fakes (hadrons misidentified as muons) which have at least four HCAL hits in the last ten planes in common with other tracks are given in function of $p_\perp$. The fraction of prompt muons which have been lost because of the inefficiencies of the algorithm treating the shadowing and the fraction of fakes which have been rejected is given in table 2.

Efficiency of the identification cuts To summarize, here are the cuts which are used in our analysis to define a muon [5]:

- $N_{exp} \geq 10$

[6]It is also possible to profit from the HCAL information making use of a sort of χ^2 test: the track is chosen for which the sum of 'residuals' (*i.e.* the distance from each hit to the extrapolated track) is smaller; however since we always require at least one muon chamber hit, this, in our case, does not help significantly in solving the ambiguity, therefore it is not used.

- $\frac{N_{fir}}{N_{exp}} \geq 0.4$
- $N_{10} > 4$
- $X_{mult} \leq 1.5$
- association of the track to *at least one* plane of the Muon Chambers
- best muon candidate in case of *shadowing* ambiguity

In addition, we apply tighter cuts with respect to those defining a "good track" for the hadronic selection, described in section 2.1, in order to ensure a good tracking quality:

- at least 5 reconstructed TPC points
- $| \cos\theta | < 0.95$
- $D_0 < 5\, mm$

where D_0 is the minimum approach distance between the track and the fitted beam centroid, in the $x - y$ plane.

Fig. 4a shows the total efficiency of these selection cuts as a function of $\cos\theta$, for Monte Carlo $Z \rightarrow \mu^+\mu^-$ events and real data; fig. 4b shows the efficiency of the HCAL cuts only.

The dips in the distribution of HCAL efficiency correspond to the barrel–endcap overlap regions, where the complicated geometry of the calorimeter causes a decrease in the resulting identification efficiency. In these regions the discrepancy between real data and Monte Carlo is due to a not perfect description of the position of the edges of the tubes in the barrel. In the barrel region ($| \cos\theta | < 0.6$) the efficiency, from real data, is not flat and in disagreement with the Monte Carlo. This is also true at low angle for the endcaps ($| \cos\theta | > 0.88$). For the barrel this discrepancy is related to readout inefficiencies in picking up the signals, and depends on the distance from the readout electronic cards. In the endcaps the discrepancy is not fully understood but there are several indications that one of the reasons is an incomplete description of the their geometry in the Monte Carlo. In the distribution of the total efficiency the two additional dips in the barrel are due to the missing Muon Chambers in the regions of ALEPH "feet". In this

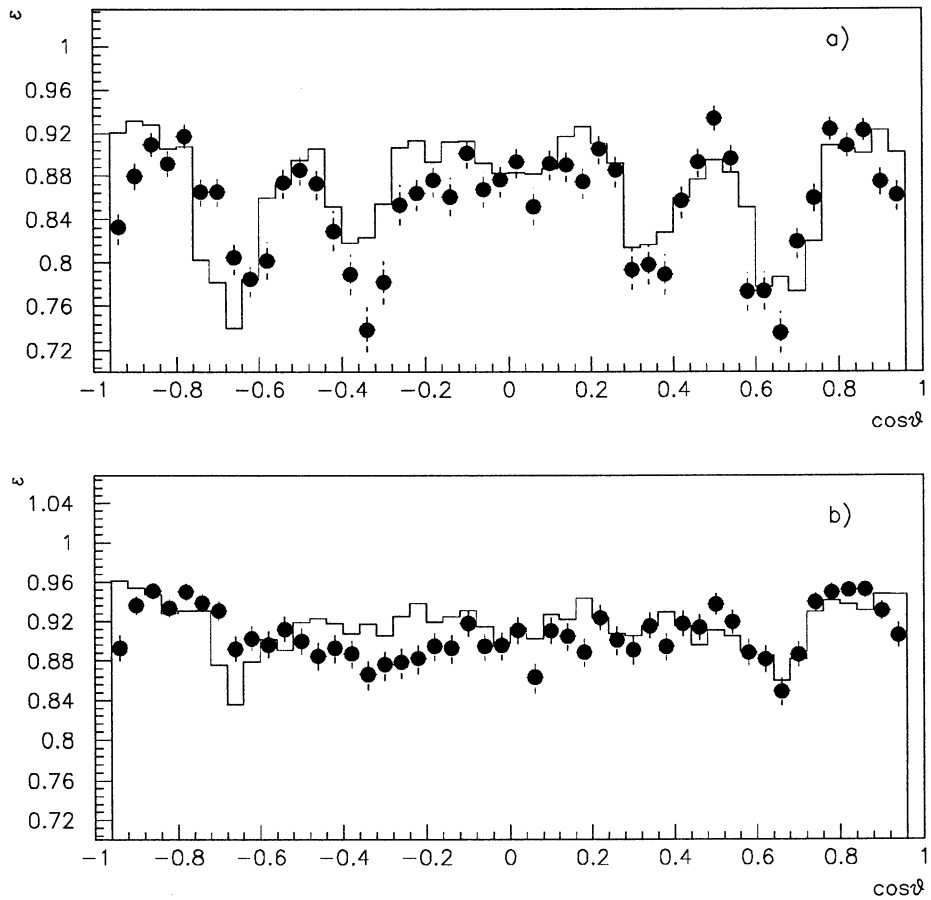

Figure 4: Efficiencies of the muon selection as a function of $\cos\theta$ with all the cuts (a) and using only HCAL (b) in 1991 data (dots) and Monte Carlo (solid line).

case the disagreement between real data and Monte Carlo is also due to the effect of the Muon Chamber efficiency simulation which does not take into account possible efficiency variations within a single chamber. Among these sources of discrepancies, the dependence of the efficiency on the position in the barrel and the improvement in the description of the overlap geometry have been simulated in the most recent Monte Carlo productions, but not in the Monte Carlo sample we have used for this analysis. For completeness in fig. 5 the effects of these modification are shown. In our analysis we have weighted the Monte Carlo events as a function of $\cos\theta$, in order to correct for the discrepancies described above.

We have verified that the muon identification efficiency is independent of momentum by selecting muons produced in τ decays. The selection is based on single–prong τ decays (not accompained by neutrals) which behave as minimum ionizing particles in the ECAL. A cut on the energy release in the HCAL towers reduces the pion contamination to a negligible level for momenta greater than 12 GeV/c (see fig. 6) [6]. In this range data and Monte Carlo are flat and in good agreement as can be seen in fig. 7. It is possible to explore the region at low momentum by using the Muon Chambers to check the HCAL identification criteria and vice versa. Since the two subdetectors are independent[7] this is a correct procedure to check the simulation of the response of the active part of these subdetectors to a muon. However in this way we do not strictly check our global identification criteria since by selecting the muon with Muon Chambers or HCAL we reject muons which do not penetrate up to the last planes of HCAL and to the Muon Chambers because of interactions with the detector. Therefore the simulation of these interactions are not fully checked with this method; on the other hand it is true that for muons they are "theoretically" well under control. Figg. 8 and 9 show, respectively, the effect of the additional requirement of at least one Muon Chamber hit and of our four HCAL cuts in our selection of muons from τ. The distributions are now flat in the whole 3 to 40 GeV/c range, and the agreement between data and Monte Carlo is good.

The jet environment can modify the efficiency of muon identification basically in two ways. As was discussed above and shown in table 2, a fraction of muons is lost because the identification is assigned to a nearby track (shadow-

[7]This is not completely true since part of the inactive zone of HCAL and Muon Chambers are overlapped

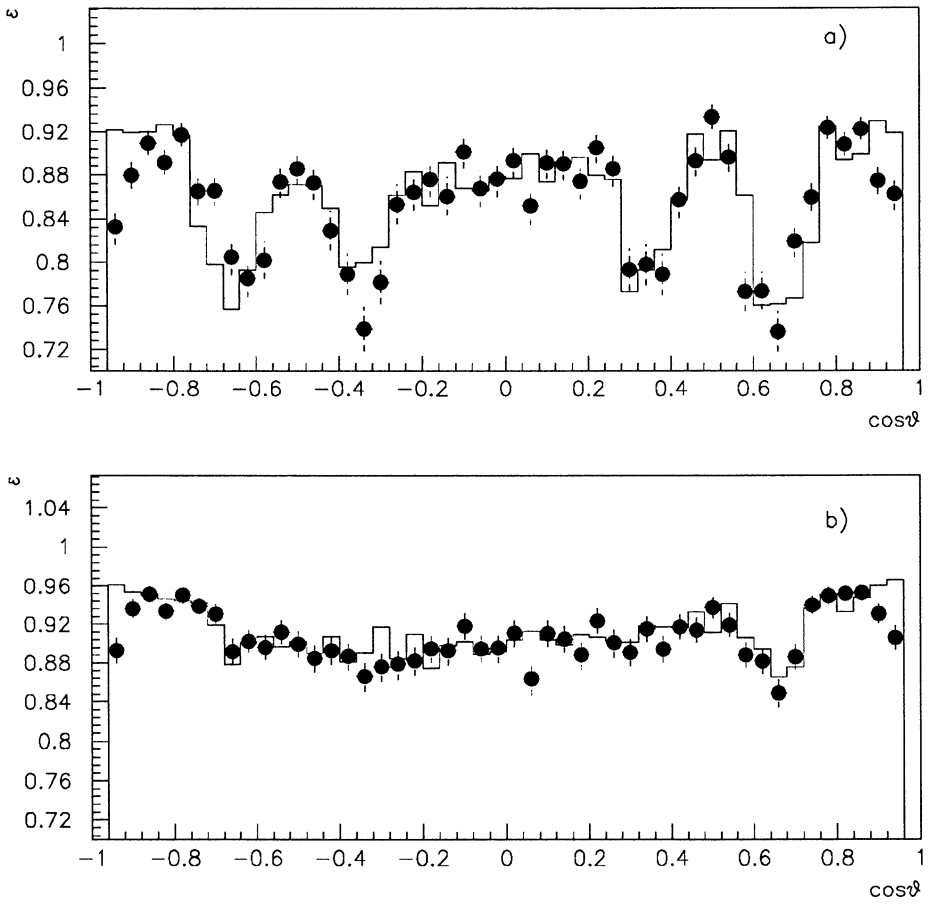

Figure 5: Efficiencies of the muon selection as a function of $\cos\theta$ with all the cuts (a) and using only HCAL (b) in 1991 data (dots) and in the new Monte Carlo (GAL 253) (solid line).

ing). This fraction, as calculated with the Monte Carlo, is very small (0.4% at low $p_\perp$) and even assuming an uncertainty of 100% on the simulation of hadronic showers (which is a rather pessimistic assumption, see the Appendix) this effect is much lower than 1%. Another way nearby hadrons can affect the efficiency is by modifying the value of N_{fir}/N_{exp}, N_{10}, X_{mult}. The behaviour of X_{mult} for pions is well simulated in Monte Carlo while discrepancies are seen in the N_{fir}/N_{exp} and N_{10} distributions (see the Appendix). We have studied the effect of N_{fir}/N_{exp} and N_{10} cuts by selecting tracks in hadronic events having hits in both muon chamber layers. This sample consists of muons with a purity of about 75%. The standard cut on N_{fir}/N_{exp} leaves $(95.4 \pm 0.4)\%$ tracks in data and $(94.9 \pm 0.5)\%$ tracks in Monte Carlo. The additional standard requirements on N_{10} and X_{mult} selects $(87.1 \pm 0.5)\%$ tracks in data and $(88.2 \pm 0.6)\%$ tracks in Monte Carlo[8]. Before drawing any conclusion out of these figures we should consider the effect due to the hadron contamination on our sample, which consists basically of pions (mostly decays) which have hit both muon chamber layers. This requirement induces a bias on the N_{fir}/N_{exp} and N_{10} distributions of these hadrons, which can be studied using the sample of pions from taus described in the Appendix. The resulting distributions are very similar to the true muon ones, therefore we conclude that the figures given above can be used for the evaluation of an upper limit on the difference in efficiency between data and Monte Carlo of about 2%.

Hadron misidentification In hadronic Z decays prompt muons are produced about one hundred times less frequently than hadrons (mostly pions), hence the muon identification algorithm has been tuned not only to identify muons with high efficiency, but also to give a very good hadron rejection power. A hadron can fake a muon by decaying to a muon itself before exiting the ALEPH Coil. This is, as far as the Hadron Calorimeter and the Muon Chambers are concerned, undistinguishable from a prompt muon. Since the lifetime and semileptonic branching ratio of pions and kaons are well known and correctly simulated by the Monte Carlo this kind of background can be easily corrected for using the Monte Carlo simulation. Hadrons can fake muons also by not interacting in ALEPH (this is called sail–through) or by

[8]The same requirements for dimuons yields $(93.6 \pm 0.2)\%$ for data and $(94.1 \pm 0.2)\%$ to be compared with $(93.8 \pm 0.5)\%$ for true muons in hadronic Monte Carlo events

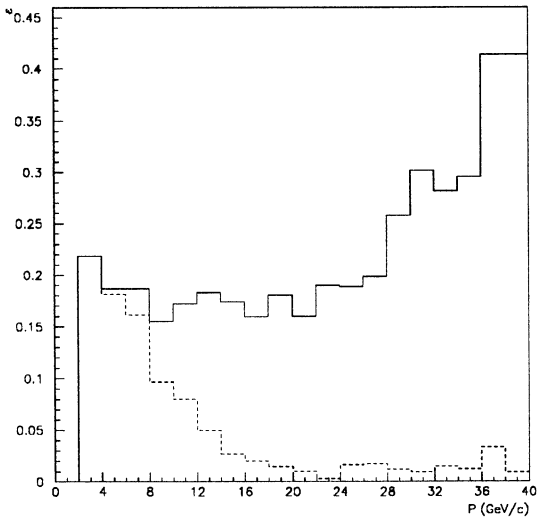

Figure 6: Pion contamination in the muon sample from τ decays selected with ECAL only (solid line) and with a 8 GeV cut on the HCAL towers energy (dashed line).

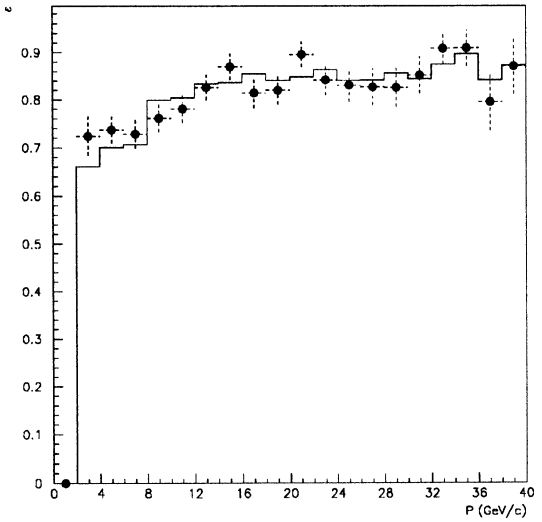

Figure 7: Efficiency of the muon id vs momentum for the τ ECAL plus HCAL towers selection. Data (dots) and Monte Carlo (solid line).

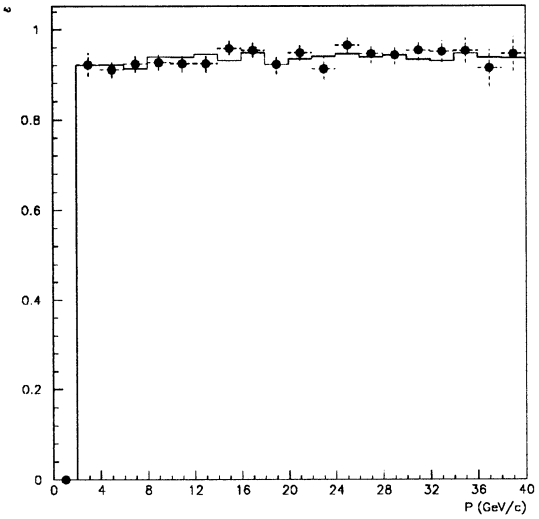

Figure 8: Efficiency of the muon id HCAL criteria vs momentum for the τ sample. Here the Muon Chambers are used to select the candidates. Data (dots) and Monte Carlo (solid line).

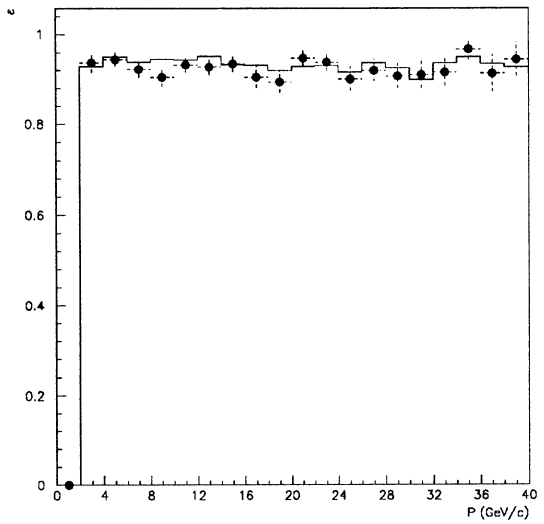

Figure 9: Efficiency of the Muon Chambers id criteria vs momentum for the τ sample. Here the HCAL is used to select the candidates. Data (dots) and Monte Carlo (solid line).

	$0 < p_\perp < 1.25$	$p_\perp > 1.25$
$3 < p < 5$	83.6 ± 1.0	86.4 ± 1.8
$5 < p < 10$	84.6 ± 1.0	84.6 ± 1.0
$p > 10$	85.1 ± 1.8	87.0 ± 0.8
total	84.2 ± 0.7	86.0 ± 0.6

Table 3: Muon identification efficiency (%) versus p and $p_\perp$in 1991 Monte Carlo.

	$0 < p_\perp < 1.25$	$p_\perp > 1.25$
$3 < p < 5$	0.16 ± 0.01	< 0.04
$5 < p < 10$	0.21 ± 0.02	0.25 ± 0.06
$p > 10$	0.15 ± 0.05	0.19 ± 0.06
total	0.18 ± 0.01	0.18 ± 0.03

Table 4: Hadron misidentification probability (%) versus p and $p_\perp$in 1991 Monte Carlo.

interacting in such a way that they are recognized as a muon by the algorithm (this is called a punch–through). The capability of the Monte Carlo to simulate the various backgrounds has been checked with data and is described in detail in the Appendix. The muon identification efficiency and the hadron rejection power of the algorithm is given (versus $p_\perp$) in table 3 and 4 for Monte Carlo $q\bar{q}$ events.

2.3 Electron identification

Electrons are identified by means of two independent measurements: the energy deposition in the Electromagnetic calorimeter, and the ionization loss (dE/dx) of the charged track in the TPC. This is described in detail in other notes ([3, 19]).

The cuts used for electron identification are summarized here:

- $R_T > -1.6$

- $-1.8 < R_L < 3.0$
- $N_{wires} > 50$
- $R_I > -2.5$

Moreover the track is discarded if it is compatible with coming from a photon conversion, *i.e.* if it satisfies the pair–rejection cuts:

- $D_{xy} < 1$ cm
- $D_z < 1$ cm
- $M_{pair} < 20$ MeV

where D_{xy} and D_z are the minimum distances in the r and z coordinates between the candidate track and any oppositely charged track in the event, while M_{pair} is their invariant mass.

In addition, the same track quality cuts as for muons are applied.

2.4 Jet clustering and $p_\perp$ definition

In this section we describe a definition of the transverse momentum $p_\perp$, which permits to reach a satisfactory purity in our b candidate sample, without losing too much in statistics.

We recall that our goal is to obtain a definition of $p_\perp$ which is as close as possible to the true transverse momentum of the lepton relative to the flight direction of the decaying heavy–flavoured hadron. The proper tuning of the jet clustering algorithm has already been discussed in [2, 3]. The same kind of studies have been performed on the new data, as far as the choice of the Energy Flow algorithm and of the y_{cut} parameter are concerned, leading to the same results.

We remind that two main strategies have been developed in ALEPH for the Energy Flow, the *Mask Algorithm* [9] and the *Calorimetric Objects Algorithm* [10, 11]. As far as our analysis is concerned, the two algorithms have proven to be essentially equivalent; we have chosen the Calobject algorithm as implemented in [11].

The clustering algorithm we use is the JADE Scaled Minimum Invariant Mass algorithm, which is generally used inside ALEPH to reconstruct jets in

hadronic events. We have fixed the value of M_{jet}, rather than that of y_{cut}, in order to make the definition independent of the centre-of-mass energy, to a value of 6 GeV/c^2. Thus our y_{cut} value is:

$$y_{cut} \equiv \frac{M_{jet}}{\sqrt{s}} = \frac{(6\ \mathrm{GeV})}{\sqrt{s}}$$

When defining the $p_\perp$ of the lepton with respect to jet axis the question arises whether or not the lepton is to be included in the computation of the jet direction. The two $p_\perp$ definitions can be written as follows:

$$\begin{aligned} p_\perp^{incl} &\equiv \frac{|\ \mathbf{p}_\ell \times \mathbf{p}_{jet}\ |}{|\ \mathbf{p}_{jet}\ |} \\ p_\perp^{excl} &\equiv \frac{|\ \mathbf{p}_\ell \times (\mathbf{p}_{jet} - \mathbf{p}_\ell)\ |}{|\ \mathbf{p}_{jet} - \mathbf{p}_\ell\ |} \end{aligned}$$

Clearly the two definitions are related by the following formula:

$$p_\perp^{excl} = p_\perp^{incl} \frac{|\ \mathbf{p}_{jet}\ |}{|\ \mathbf{p}_{jet} - \mathbf{p}_\ell\ |} \equiv p_\perp^{incl} \mathcal{F}_{incl}^{excl}$$

The $p_\perp$cut is basically aimed to rejecting *physical* backgrounds ($b \to c \to \ell$ and $c \to \ell$), since the background due to misidentified hadrons is only weakly related to $p_\perp$.

The main feature of the $p_\perp^{excl}$ definition with respect to the other is that it allows a better rejection of $b \to c \to \ell$ background, since in this case we have a lepton which is, on average, less energetic than in the $b \to \ell$ case, while the jet is of the same kind. On the other hand, charm jets have, on average, a lower particle multiplicity than beauty jets, which can sometimes cause $\mathcal{F}_{incl}^{excl}$ to have a high value, leading to a higher charm contamination.

For this reason the choice of the $p_\perp$ definition is strongly dependent on the algorithm chosen for the calculation of the jet direction; in particular the use of an Energy Flow algorithm greatly improves the determination of the jet direction for charm events.

We have studied the efficiency of the selection *vs.* the purity for the two $p_\perp$ definitions, using the Energy Flow algorithm. For the *single lepton* sample we get fig. 10 where the efficiency is defined as the number of detected $b \to \ell$ decays divided by the total number of $Z^0 \to b\bar{b}$ decays. We get, as expected,

a much lower $b \to c \to \ell$ contamination, while, in the central region, the $c \to \ell$ contamination is a little bit higher. The resulting signal $(b \to \ell)$ purity is higher with the $p_\perp^{excl}$ definition. (Our selected cut will correspond to an efficiency of about 15%).

For the *dilepton* sample where $b \to c \to \ell$ is the only relevant background, the $p_\perp^{excl}$ definition is clearly better. For example, if we assume that with our final $p_\perp$ cut we have a probability of selecting a $b \to \ell$ of 70%, and a probability of selecting either a $b \to c \to \ell$ or a $c \to \ell$ around 7%, requiring two leptons, we get a charm contamination of ≈ 0.5 %, while the $b \to c \to \ell$ will contribute basically through $(b \to \ell)$ $(b \to c \to \ell)$ events by $\approx 10\%$.

Fig. 11 shows the $(b \to \ell)$ $(b \to c \to \ell)$ and $(c \to \ell)$ $(c \to \ell)$ fractions for various cuts in the *dilepton* sample, and the corresponding signal purity. Here the efficiency is defined as the number of detected $(b \to \ell)$ $(b \to \ell)$ decays divided by the total number of $Z^0 \to b\bar{b}$ decays. Similar results are shown in [18].

From now on we shall use the $p_\perp^{excl}$ definition [9]; the exact value of the cut has been decided after a separate study for the asymmetry and for the mixing analyses, aimed at finding the cut value which minimizes the final statistical error. It was found that a cut at $p_\perp > 1.25$ is satisfactory for both analyses. Details about the study on the $p_\perp$ cut will be given below.

2.5 Summary of Selection Cuts

To summarize, here are the steps of our b selection procedure (see also [7]):

- hadronic events are selected through the cuts described in section 2.1
- each hadronic event is split up into jets according to the Scaled Minimum Mass algorithm, making use of Energy Flow objects, and requiring $M_{jet} = 6$ GeV/c^2. The event must contain at least two jets
- events where the lepton carries more than 90% of the jet momentum, or where the jet containing the lepton is made by less than 3 "objects"

[9] In our previous analysis we used [1, 2] $p_\perp^{incl}$ for the asymmetry, with a mixing value obtained using charged tracks and $p_\perp^{excl}$ [21]. This was done in order to have the lowest possible contamination from $c \to \ell$. Since then the Energy Flow algorithm has improved and as we can see in fig. 10 the two definitions are equivalent as far as the charm contamination is concerned, for the cut we have chosen. This allows the use of the same $p_\perp$ definition for mixing and asymmetry.

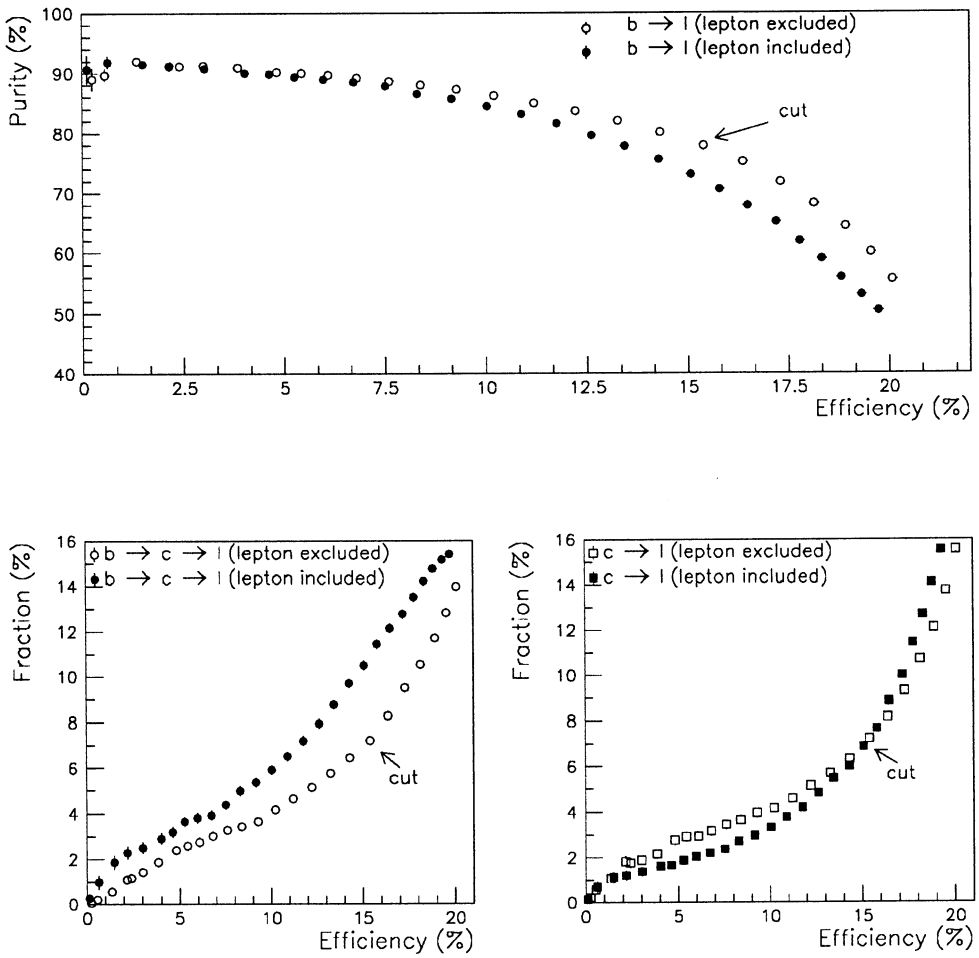

Figure 10: Purity and contaminations *vs.* efficiency in the single lepton sample.

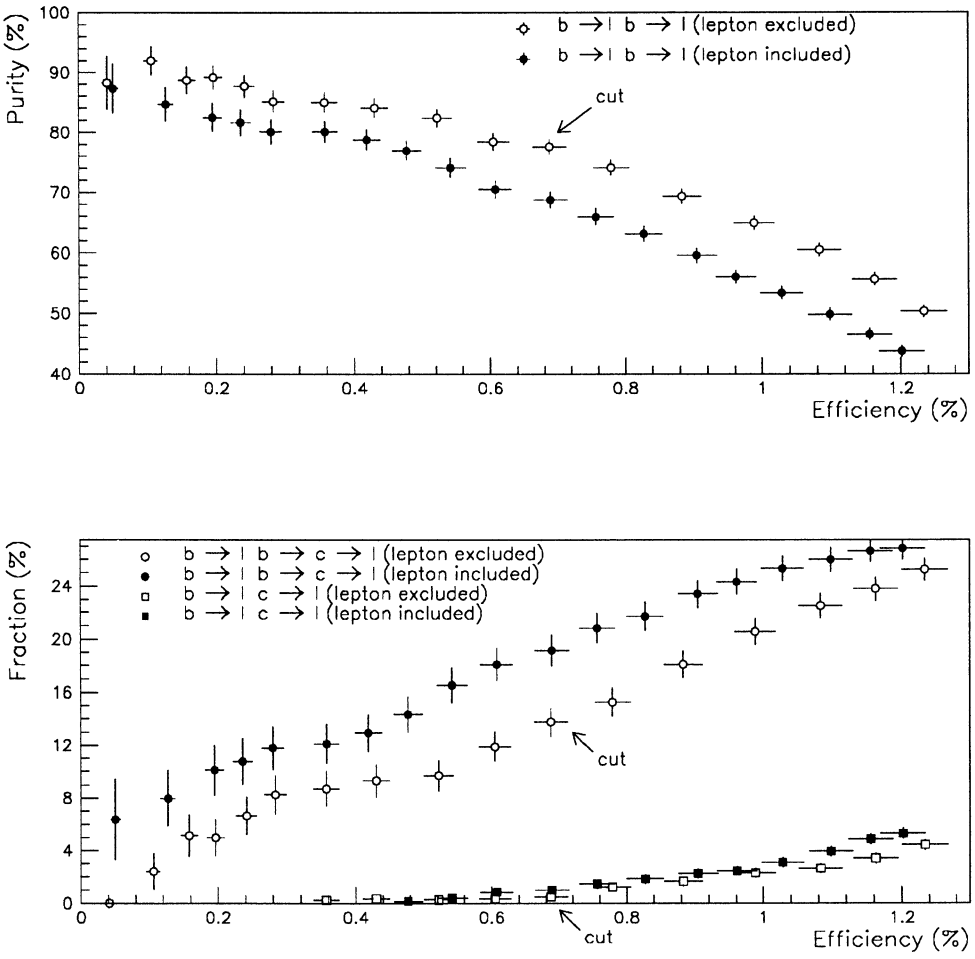

Figure 11: Purity and contaminations *vs.* efficiency in the dilepton sample

are discarded. The purpose of this is the rejection of those events where the jet clustering algorithm makes a jet containing one energetic lepton together with some very soft fragmentation products

- the event is kept if at least one lepton (electron or muon) is detected whose momentum, p, and transverse momentum with respect to the jet it belongs to, $p_\perp$, satisfy the following conditions:

$$p > 3\ \mathrm{GeV/c} \quad (1)$$
$$p_\perp > 1.25\ \mathrm{GeV/c} \quad (2)$$

3 Measuring the Asymmetry

3.1 Fit of the Raw Asymmetry

Given our sample of candidate $Z^0 \to b\bar{b}$ events, our purpose is the determination of the angular distribution of the lepton's parent quark. The quark's direction is approximated by the thrust axis of the event,which is reconstructed starting from Energy Flow objects. The direction and the charge of the lepton can be used to tell which of the two possible orientations of the thrust axis represents the emission direction of the b quark. The procedure is the following:

- the vector momentum of the jet which includes the negative lepton is computed, by taking into account all the tracks and the Energy Flow objects the jet is made of, *including* the lepton

- the orientation of the global thrust axis is chosen so that it makes an angle less than 90° with the jet momentum. The thrust axis direction is described by the polar angle θ

- the thrust axis orientation determined with the above criterion is reversed if the lepton charge is positive (which — in the ideal case — means that the jet originated from the decay of a $\bar{b}$). This can be expressed by

$$\cos\theta = -Q \cdot \cos\theta_{thrust} \quad (3)$$

where Q is the lepton charge.

By this procedure we uniquely define $\cos\theta$ for each event, so we can proceed to measure the angular distribution.

Fig. 12 shows the distributions for the 1990 and 1991 samples separately, as well as for the electrons and muons; the angular distribution of the total sample is shown in fig. 13.

In each of these plots, the first and the last bin show the effect of the lower acceptance at small polar angles.

The asymmetry value is extracted via a fit to the angular distribution:

$$\frac{d\sigma}{d\cos\theta} = C(1+\cos^2\theta + \frac{8}{3}A_{FB}^{obs}\cos\theta) \tag{4}$$

where the factor $8/3$ comes in to let the definition of A_{FB} match with the traditional one

$$A_{FB} = \frac{N_F - N_B}{N_F + N_B} \tag{5}$$

The fit procedure used is the *Maximum likelihood* method, which is unbinned, *i.e.* the full information on $\cos\theta$ is used for each event.

Another advantage of this fitting procedure is that one can disregard the effect of any multiplying constant in the probability density expression. Indeed, such a scaling factor becomes an additive constant which doesn't affect the result of the minimization procedure. Actually, this is true for any correction function which is not dependent on the parameters, such as an acceptance function $\epsilon(x)$: since no contribution to the partial derivative $\partial l/\partial a$ comes from such a piece in the log-likelihood sum, it doesn't affect the minimization (*i.e.* the fit) result.

3.2 Effect of acceptance weights

Due to its geometrical structure, which is far from being spherically symmetric, the ALEPH detector's response is not exactly uniform along the polar angle range. This obviously reflects into an angular non-uniformity for all kinds of event selection and particle identification. Such effects are generally small but they need to be investigated.

The most straightforward way of correcting for non-uniformities is to determine a correction function from Monte Carlo: if the simulation program predicts an efficiency function $\epsilon(\theta)$, then $f(\theta) = 1/\epsilon(\theta)$ is the correction function one looks for. It is convenient to define such a function as a set of

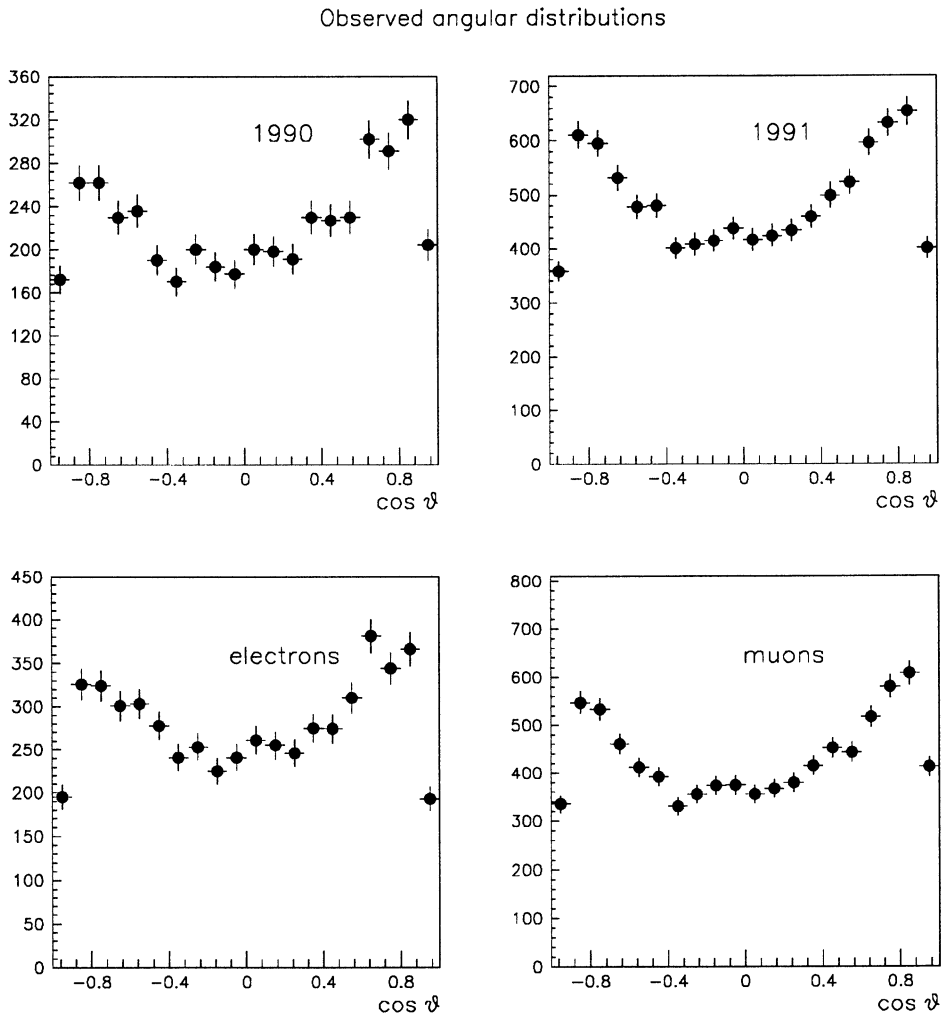

Figure 12: Observed angular distributions separately shown for the total 1990 and 1991 samples, as well as for the total electron and muon samples, at the peak energy.

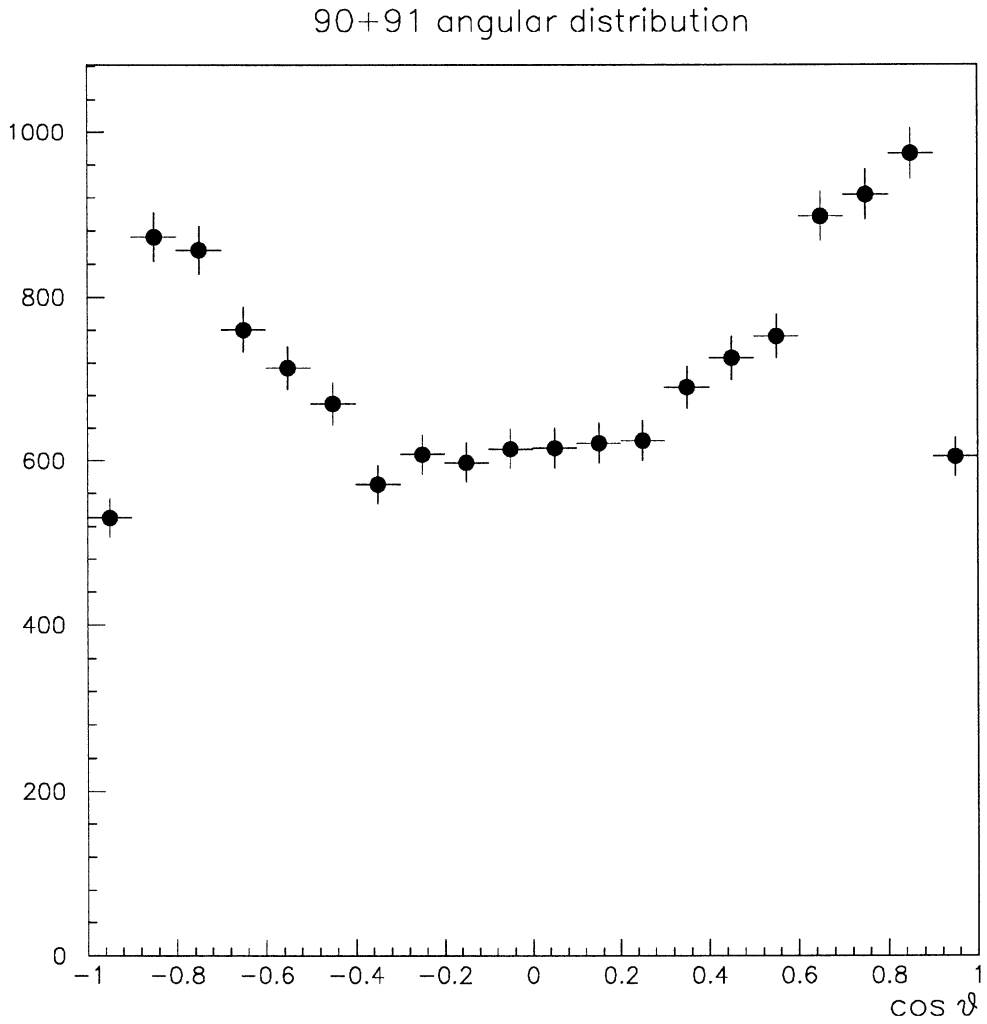

Figure 13: Observed angular distribution for the total 1990 + 1991 sample.

weights, to be applied each to a bin of the angular range. This is only done for practical purposes since, as was stressed above, our fitting procedure does not require binned data.

For each $\cos\theta$ bin i, one can write

$$W_i = \frac{n_i^{true}}{n_i^{rec}} \tag{6}$$

where n_i^{true} and n_i^{rec} are respectively the number of Monte Carlo $Z^0 \to b\bar{b}$ events where the direction of the thrust axis is contained in the i-th $\cos\theta$ bin, and the number of reconstructed events in the same bin.

Such a correction function is in general forward–backward asymmetric, as was seen before. Anyway, if we look at our specific case, where events are naturally symmetrized by the charge–flavour correlation procedure, we see that our acceptance correction function is eventually symmetrical, independently of the value of the asymmetry itself, as long as the selection efficiency is the same for positive and negative tracks.

To show this, let's consider the simplified case of two bins (forward–backward direction).

Suppose the apparatus has an asymmetrical acceptance, described by the two efficiencies ϵ_F and ϵ_B. Since we reverse the sign of $\cos\theta$ for events with positive leptons, we get

$$\begin{aligned} N_F^{rec} &= \epsilon_F N_F^- + \epsilon_B N_B^+ \\ N_B^{rec} &= \epsilon_B N_B^- + \epsilon_F N_F^+ \end{aligned}$$

Knowing that

$$N_F = N\frac{1+A_{FB}}{2}, \quad N_B = N\frac{1-A_{FB}}{2}$$

one has

$$\begin{aligned} N_F^{rec} &= \frac{1+A_{FB}}{2}(\epsilon_F N^- + \epsilon_B N^+) \\ N_B^{rec} &= \frac{1-A_{FB}}{2}(\epsilon_B N^- + \epsilon_F N^+) \end{aligned}$$

If

$$N^+ = f^+ N_{tot}, \quad N^- = f^- N_{tot}$$

we have

$$\begin{aligned} N_F^{rec} &= N\frac{1+A_{FB}}{2}(\epsilon_F f^- + \epsilon_B f^+) \\ N_B^{rec} &= N\frac{1-A_{FB}}{2}(\epsilon_B f^- + \epsilon_F f^+) \end{aligned}$$

We see that if $f^+ = f^-$, which is a reasonable assumption as long as there are no serious problems with the tracking detector, the two acceptance factors (those between brackets) are exactly equal.

Due to limited available Monte Carlo statistics, fluctuations can create a fake asymmetry, when computing the weights according to eq. 6.

We note, however, that if we sum the angular distributions for positive and negative tracks *without* reversing the direction for the positive case, the two samples being on average equal, we expect exactly a $1+\cos^2\theta$ distribution for the data. Therefore if we define

$$W_i = C\frac{n_i^{neg} + n_{-i}^{pos}}{1+\cos^2\theta_i}$$

where

$$C = \frac{3}{8}\sum_i N_i + N_{-i}$$

is the normalization factor, we get a set of 'naturally' symmetrized weights where whe have cancelled out the effects due to the asymmetric angular distribution of data themselves. This definition also has the advantage of being less sensitive to fluctuations, the denominator being a function and not a stochastic object. With this procedure we still have weights which are in principle asymmetric, but whose asymmetry is only due to the apparatus acceptance, as it is implemented in the simulation code. To go back to the previous example, our weights are now the equivalent of ϵ_F and ϵ_B. However, as we said above, an asymmetry can also be created by the statistical fluctuations between the positive and negative track samples in our Monte Carlo data.

We can then decide to have symmetrical weights in practice and not only in principle, symmetrizing them by hand and defining:

$$W_i = W_{-i} = \frac{n_i^{true} + n_{-i}^{true}}{n_i^{rec} + n_{-i}^{rec}}$$

where i and $-i$ are symmetrical bins with respect to $\theta = \pi/2$.

We have used both the symmetrized and the unsymmetrized set of weights in the evaluation of the raw asymmetry, and we saw no appreciable difference in the result, as was to be expected from the arguments above.

It turns out that in order to work properly, these weights have to be normalized, and the normalization condition is that they conserve the total number of events, *i.e.*

$$\sum_i W_i = N_{bins}$$

This condition fixes the value of the constant C.

The way such weights enter the likelihood funcion is the following:

$$\mathcal{L} = \prod_i \prod_{k \in i} f_i(\cos\theta)^{W_i} \tag{7}$$

where the second product is extended to all the events contained in bin i.

To explain why it must be so let's suppose the data are binned. In that case the effect of weights is to change the measured population of the i-th bin by the corresponding computed factor. Thus the likelihood function must change to

$$\prod_i f(\cos\theta_i)^{n_i^{true}} = \prod_i f(\cos\theta_i)^{n_i^{rec} W_i} = \prod_i \prod_{k \in i} f(\cos\theta_k)^{W_i} \tag{8}$$

where the last expression is equal to eq. 7. One can easily see that eq. 7 still holds for unbinned data, if one substitutes the discrete weights W_i with a continuous correction function. The use of discrete values is however a good approximation.

It is now clear why it's important to have the weights normalized to give unit average. Changing such a normalization would artificially change the total number of events, and therefore cause the evaluation of the statistical error to be inadequate.

The acceptance weights have been calculated from our Monte Carlo sample, choosing a bin size of 0.05 in $\cos\theta$: their values are plotted in fig. 14. The value at the edge of the angular range ($|\cos\theta| > 0.95$) is high due to losses at small angles. This small–angle range has been excluded from the fit. As one can see, apart from this edge effect, the weights are fairly constant and they can be expected to have little effect on the asymmetry measurement. Indeed, we explicitly verified that the central value of the fit remains the

same within a small fraction of the statistical error. This is also true for the muon and elecron samples separately.

In addition to the set of weights determined from Monte Carlo alone, we have also employed lepton identification correction factors, determined from the comparison of real data angular distributions to Monte Carlo (see lepton identification sections). Such weights are a function of $\cos\theta$ for muons, while they are given as a function of $\cos\theta$, p and $p_\perp$ for electrons. These weights have been applied to the events according to the direction and the momentum of the detected lepton. Again, no effect can be seen on the result of the fit.

The main effect of acceptance weights is therefore the "esthetical" improvement of the angular distribution plot of fig. 16.

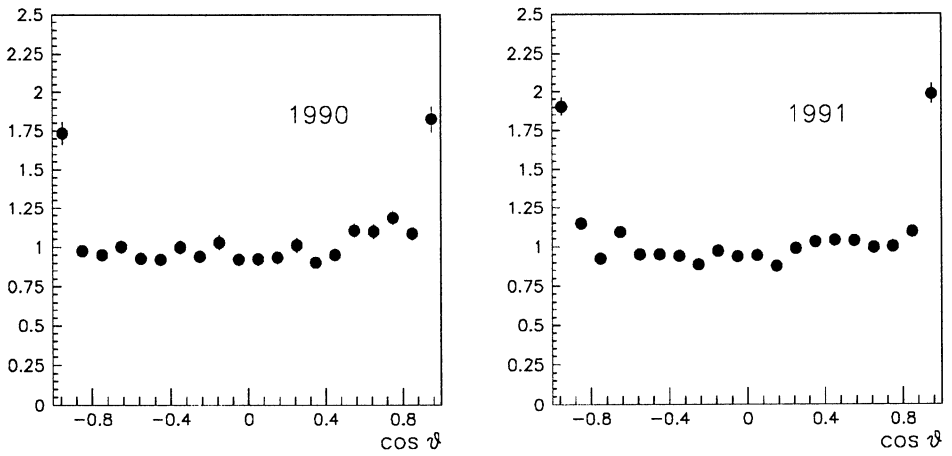

Figure 14: Acceptance weights for the total lepton sample in 1990 and 1991, determined from Monte Carlo.

3.3 Results of the fit

The hadronic events we used for the fit are the full statistics collected in 1990 and 1991 consisting in about 148200 $Z^0 \to q\bar{q}$ for 1990 and 285800 $Z^0 \to q\bar{q}$ for 1991.

Fig. 15 shows the number of events which pass our $Z^0 \rightarrow b\bar{b}$ selection cuts, at the various beam energies, both in 1990 and 1991.

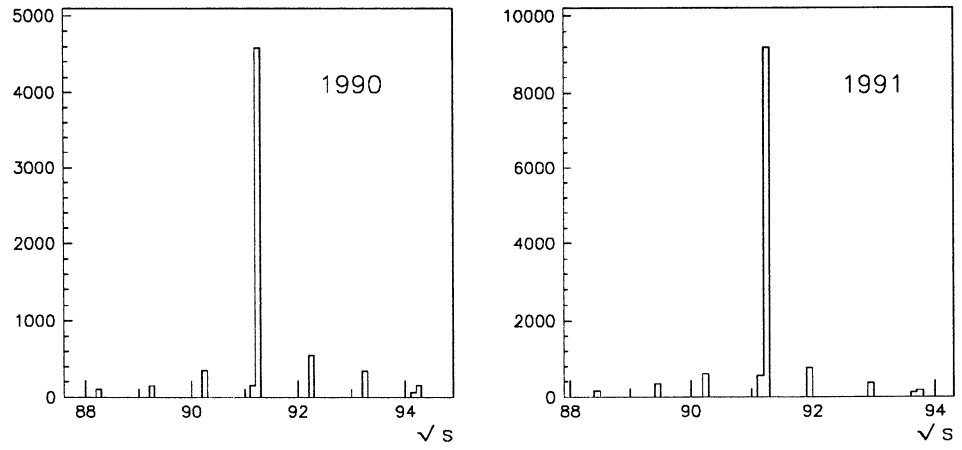

Figure 15: Distribution of selected events at the various centre-of-mass energies, for both years.

The minimization of the log–likelihood function is performed using the MINUIT standard program [27].

The results of the fit, separately computed for the electron and muon sample, as well as for the total sample, are shown in table 5.

The fitted curve is shown in fig. 16, for the total sample, at the peak energy.

Table 6 shows the results of the fits at the seven energy points, for the total sample.

3.4 Extraction of $A_{FB}(b)$

The reason why the observable forward–backward asymmetry A_{FB}^{obs} differs from the 'true' b asymmetry $A_{FB}(b)$ is twofold:

1. the sample is contaminated by various background sources, that is, a fraction of the selected events was not due to $Z^0 \rightarrow b\bar{b}$ decays

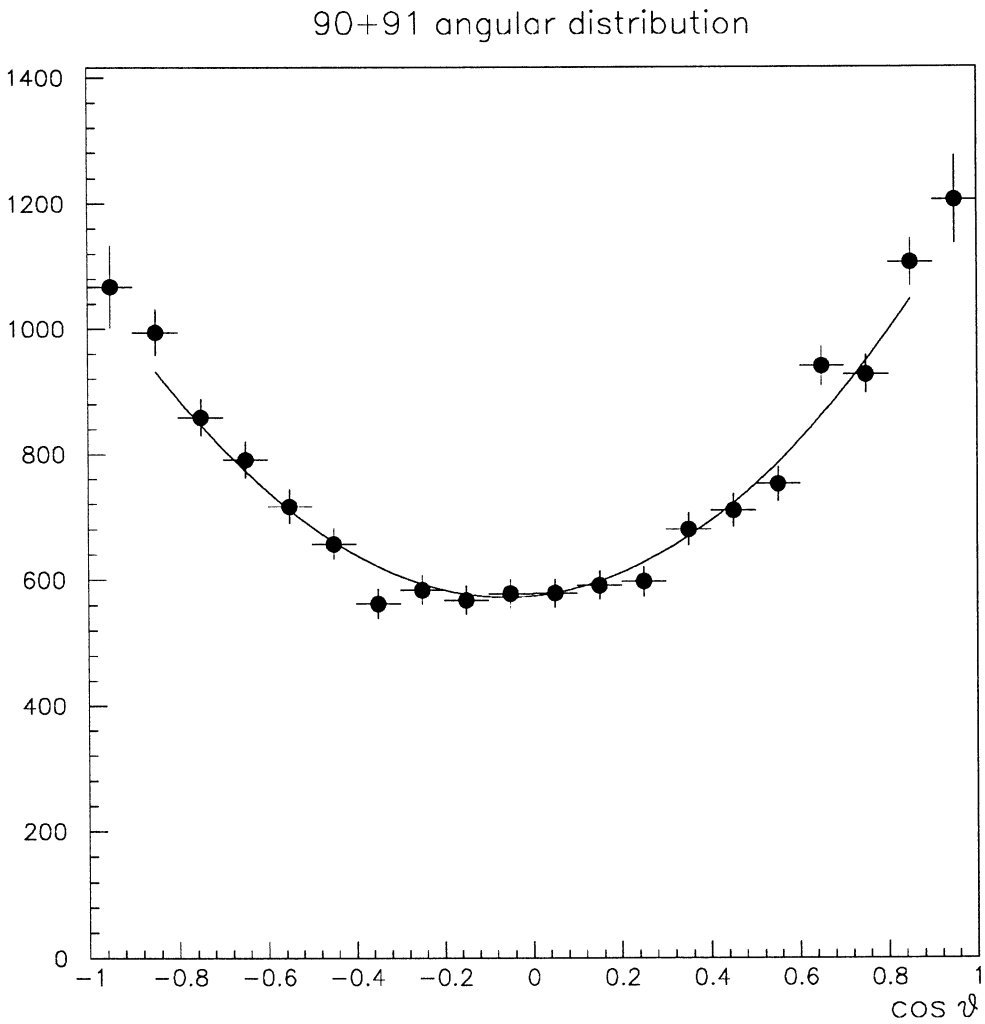

Figure 16: Observed angular distribution for the total 1990 + 1991 sample, with the fitted curve superimposed.

Tagging lepton	Year	Raw asymmetry (%)
e	1990 + 1991	4.3 ± 1.4
μ	1990 + 1991	4.8 ± 1.1
$e + \mu$	1990	6.8 ± 1.5
$e + \mu$	1991	3.6 ± 1.0
Total sample		4.5 ± 0.9

Table 5: Values of the fitted raw asymmetry at the peak, separately for the 1990, 1991 and total sample, and for the electron and muon samples. The errors are statistical only.

Energy Point	Fitted Asymmetry (%)
Peak - 3 GeV	3.9 ± 6.3
Peak - 2 GeV	-0.9 ± 4.7
Peak - 1 GeV	2.8 ± 3.3
Peak	4.5 ± 0.9
Peak +1 GeV	4.1 ± 2.9
Peak +2 GeV	7.1 ± 3.8
Peak + 3 GeV	8.5 ± 4.5

Table 6: Values of the fitted raw asymmetry at seven energy points for the total sample. The errors are statistical only.

2. for a certain fraction of the detected $Z^0 \to b\bar{b}$ events the correlation between the lepton charge and the quark flavour is not the expected one, either because of $B^0\bar{B}^0$ mixing or because of the contamination from $b \to c \to \ell$ ("cascade") events, where the charge is anticorrelated with the quark flavour.

To see how the latter effect works, suppose we have a pure sample of $b \to \ell$ events, for a fraction χ of which, the charge of the tagged lepton has the wrong sign with respect to the expected one, due to the fact that the B meson has turned to a $\bar{B}$ (or *vice versa*). This causes the cosine of the polar angle θ to be taken with the wrong sign. This implies

$$N_F^{meas} = N_F^{true} \cdot (1-\chi) + \chi \cdot N_B^{true}$$

$$N_B^{meas} = N_B^{true} \cdot (1-\chi) + \chi \cdot N_F^{true}$$

As a result

$$A_{FB}^{meas} \equiv \frac{N_F^{meas} - N_B^{meas}}{N_F^{meas} + N_B^{meas}} = (1-2\chi)A_{FB}^{true}$$

The fraction from "cascade" events simply contributes in the same way but with a reversed sign. We note, however, that some of the "cascade" events are actually events where the virtual W emitted by the b quark decays to a $\bar{c}s$ couple, followed by the semileptonic decay of the $\bar{c}$ quark. These events have the "right" charge–flavour correlation.

We can now write down the relation between the observed and the true b asymmetry given the fractional composition of the sample and the mixing parameter χ.

$$A_{obs} = (1-2\chi)(\eta_{right} - \eta_{wrong})A_{FB}(b) - \eta_{c\to l}A_{FB}(c) + \eta_{bkg}A_{bkg} \qquad (9)$$

where

$$\begin{aligned} \eta_{right} &\equiv \eta_{b\to\ell} + \eta_{b\to\tau\to\ell} + \eta_{b\to\bar{c}\to\ell} \\ \eta_{wrong} &\equiv \eta_{b\to c\to\ell} \end{aligned}$$

and η_i is the fractional contribution of process i to the final sample composition. A_{bkg} is the "residual" asymmetry due to the background processes.

Event type	Sample fraction (%)			
	1990		1991	
	e	μ	e	μ
$b \to \ell$	82.2 ± 0.6	73.1 ± 0.7	82.4 ± 0.4	72.8 ± 0.3
$b \to \tau \to \ell$	1.2 ± 0.2	1.3 ± 0.2	1.2 ± 0.1	1.1 ± 0.1
$b \to c \to \ell$	6.1 ± 0.4	6.2 ± 0.4	6.1 ± 0.2	6.2 ± 0.2
$b \to \bar{c} \to \ell$	0.4 ± 0.1	0.3 ± 0.1	0.3 ± 0.1	0.4 ± 0.1
$c \to \ell$	5.3 ± 0.4	5.7 ± 0.3	5.3 ± 0.2	6.0 ± 0.2
$K, \pi \to \mu$	—	7.6 ± 0.4	—	8.0 ± 0.2
$\gamma \to e^+e^-$	1.0 ± 0.2	—	1.5 ± 0.1	—
misid. hadron	1.0 ± 0.2	3.7 ± 0.3	0.9 ± 0.1	3.5 ± 0.1

Table 7: Sample composition for the various data selections.

The minus sign in front of the charm contribution takes into account the fact that leptons from direct charm decay have the 'wrong' charge with respect to our convention.

We see from eq. 9 that it is possible to solve for $A_{FB}(b)$, as long as we possess reliable predictions on all the quantities entering the equation.

The composition fractions η_i are determined through Monte Carlo simulation.

The events have been selected using the cuts described in section 2.5 and the resulting sample compositions for the two years and for the two lepton species are shown in table 7.

We are left with the non–b asymmetries $A_{FB}(c)$ and A_{bkg}: we take the latter from our Monte Carlo sample, considering those kind of backgrounds which are not intrinsically symmetric, which is the case for instance for electrons coming from a converted photon, or for leptons coming from the decay of a J/ψ. The Monte Carlo predicts that such background is basically due to decays and misidentified hadrons. A residual asymmetry in these events is due to the *leading particle* effect, which induces a correlation between the selected particle's charge and the charge of the parent quark.

In order to reduce the disadvantages due to poor statistics, we decided to study the background asymmetry by selecting a Monte Carlo background sample where the lepton identification cuts have been released. The flavour

composition of the sample thus selected is very similar to that of the decays and misidentified hadron part of our Monte Carlo "lepton" sample. In both samples one can see that the kinematical cuts enhance the b flavour component. The predicted asymmetries for each flavour, from the "hadron" sample, have then been reweighted according to the flavour composition of the "lepton" sample. We get

$$A_{bkg} = (1.4 \pm 0.7)\%$$

As to the charm asymmetry, we decided to rely on the Standard Model only as far as the ratio between charm and beauty asymmetries is concerned. The reason for this is that the ratio

$$\kappa = \frac{A_{FB}(b)}{A_{FB}(c)}$$

is well predicted by the Standard Model with almost no dependence on the top mass.

So, if we put

$$A_{FB}(b) = \kappa A_{FB}(c)$$

we can solve eq. 9 to get

$$A_{FB}(b) = \frac{A^{obs} - f_{bkg}\eta_{bkg}A_{bkg}}{(1-2\bar{\chi})(\eta_{right} - \eta_{wrong}) - \frac{1}{\kappa}\eta_{c\to l}} \tag{10}$$

The results are summarized for various subsamples in table 8.

3.5 Evaluation of the systematic errors

The possible sources of systematic errors in the measurement of $A_{FB}(b)$ can be divided into two categories: those which directly affect the observed angular distribution, and hence the value of the raw asymmetry, and those which affect the quantities appearing in eq. 10, thus causing a bad evaluation of what we call the *true* asymmetry.

The first category includes acceptance effects, which turn out to be very small, and errors in the determination of the quark axis direction, due to the choice of a particular clustering algorithm and jet definition.

The second category turns out to be the more relevant one, at least to our level of understanding.

sample	$A_{FB}(b)$(peak) (%)
e (1990+1991)	7.9 ± 3.0
μ (1990+1991)	8.8 ± 2.3
e+μ (1990)	12.1 ± 2.9
e+μ (1991)	6.2 ± 2.0
total sample	7.9 ± 1.6

Table 8: Values of the extracted $A_{FB}(b)$ at the Z peak separated by tagging lepton as well as by year. The errors are statistical only.

Energy Point	κ
Peak -3 GeV	-0.18
Peak -2 GeV	-0.67
Peak -1 GeV	10.0
Peak	1.3
Peak +1 GeV	1.1
Peak +2 GeV	0.91
Peak +3 GeV	0.83

Table 9: Values of the ratio κ at the various energy points, from Expostar.

Eq. 10 contains the sample fractions, which we take from Monte Carlo, the ratio k between $A_{FB}(b)$ and $A_{FB}(c)$, and the mixing parameter $\bar{\chi}$, which we measure directly from data.

The values for κ used at the various energy points are taken from Expostar [13], and are listed in table 9.

The sample fractions have been determined on the basis of a finite sample of Monte Carlo data, and thus have a statistical error. They also suffer from systematics due to their implicit dependence on various physical parameters such as the semileptonic branching ratios of heavy quarks and fragmentation parameters.

Knowing what values have been used in the Monte Carlo, we can study the effect on the sample composition, and consequently on the extracted

asymmetry, induced by a shift in each of these parameters. We can then correct the raw Monte Carlo prediction for the sample composition, by shifting each parameter to the chosen value; then, in order to obtain an estimate for the systematic error due to the poor knowledge of that particular parameter, we can determine the effect on our final result induced by a variation of the parameter by plus or minus one sigma.

Since the sample composition fractions are all correlated (their sum is unity), a variation of each physical parameter will affect all of the sample fractions. For instance, supposing

$$\mathrm{BR}(b \to \ell) \to (1+\epsilon)\mathrm{BR}(b \to \ell)$$

then one will have that, to first order

$$N_{b\to\ell} \to (1+\epsilon)N_{b\to\ell}$$

where N_i is the number of selected events belonging to the i-th species. Now we can easily see that every fraction η_i will be affected by such a variation, since $N_{b\to\ell}$ is contained at least in the denominator:

$$\eta_i = \frac{N_i}{\sum_k N_k}$$

The sources of systematics we have considered, that is to say the parameters we have varied, are the following:

- the semileptonic branching ratio of the b and c quarks

  $$\mathrm{BR}(b \to \ell),\ \mathrm{BR}(c \to \ell)$$

- the "cascade" branching ratio

  $$\mathrm{BR}(b \to c \to \ell)$$

  which we take as an independent quantity, with respect to the branching ratio product $\mathrm{BR}(b \to c) \cdot \mathrm{BR}(c \to \ell)$. To explain this choice, we note that the production composition of charmed mesons in the $b \to c \to \ell$ events is not necessarily the same as for $c \to \ell$ production. The lepton spectrum will then be different for the two event species,

and therefore a small change of the average $c \to \ell$ branching ratio would not have te same effect on the number of selected primary c and cascade events. The two processes are indeed correlated to a certain extent, and therefore we decided to treat them as completely correlated when computing the error propagation, in order to stay on the conservative side

- the branching fraction BR($b \to W \to \bar{c} \to \ell$)
- the branching fraction BR($b \to \tau \to \ell$)
- the value of Γ_b
- the fragmentation parameters ε_b and ε_c of the heavy quarks, as they appear in the Peterson parameterizing function. For the fragmentation of the b quark, we have also studied the effect of the use of a different fragmentation model, namely the Kartvelishvili model. [29]

The semileptonic decays of the B hadrons are generated in the Monte Carlo according to the Altarelli model [24]. However, the data from lower energy experiments (CLEO, ARGUS) can also easily be fitted to a different model by Isgur, Scora, Grinstein and Wise with the total D^{**} fraction of $b \to \ell$ set to 32% (we will refer to it as the ISGW model) which predicts a softer lepton spectrum [25]. An incorrect description of the lepton spectrum can of course affect our results, by changing the sample composition resulting from the p, $p_\perp$ cuts.

Therefore, we have considered, as a further source of systematics, a possible model dependence of our results, changing the spectrum shape from the Altarelli to the ISGW model.

To extract the value of $A_{FB}(b)$ using the ISGW model for the lepton spectrum, for consistency reasons we have to make use not only of the slightly different sample composition that we get having softened the spectrum, but also of the different results for the $b \to \ell$ and $b \to c \to \ell$ branching ratios which are found when this model is assumed, as well as the slightly different result for the mixing parameter (see sect. 4.4) .

We find that the central value of the extracted asymmetry decreases by 0.05 (expressed in percent), leaving the result practically unchanged:

$$A^b_{ISGW} = (7.9 \pm 1.8 \pm 0.8)\% \tag{11}$$

	MC (%)	Altarelli (%)	ISGW (%)
$b \to \ell$	10.4	$11.4 \pm 0.3 \pm 0.3$	$11.8 \pm 0.3 \pm 0.3$
$b \to c \to \ell$	9.9	$8.7 \pm 0.3 \pm 0.6$	$7.5 \pm 0.2 \pm 0.6$

Table 10: Fitted values for the $b \to \ell$ and $b \to c \to \ell$ branching ratios, compared to the Monte Carlo values.

The values of the branching ratios $b \to \ell$ and $b \to c \to \ell$ have been taken from the ALEPH fit results [19], separately for the Altarelli and the ISGW models. The values we have used, together with the Monte Carlo values, are listed in table 10.

For the $b \to \ell$ branching ratio, we have also taken into account the contribution due to the uncertainty on the fraction of events coming from $b \to u$ transitions [22], which has been varied by 50%.

The $b \to \tau \to \ell$ branching ratio has been taken from the latest ALEPH measurement [26].

The branching fraction BR($b \to W \to \bar{c} \to \ell$) has been varied by about 70 % (where we have summed in quadrature a 50 % variation accounting for the uncertainty on the branching ratio, with a further 50 % variation acconting for model inadequacy).

As to the $c \to \ell$ branching ratio, we decided to keep the Monte Carlo value [23] and vary it by $\pm 15\%$.

The Γ_b has been conservatively set to 5%, without shifting the Monte Carlo value, which is equal to the Standard Model prediction.

The variation of the sample fractions have been calculated assuming that changing one of the above branching ratios would only affect the number of detected events for the corresponding species, leaving the other species unaffected.

The effect of a change in the lepton spectrum, either due to changing the decay model, or the heavy quark fragmentation parameters, has been estimated using the following technique: since a variation of the fragmentation parameter ε translates into a change of shape for the distribution of the fragmentation variable z, for each Monte Carlo event the value of z which was used to generate the event is extracted, and the event is given a weight which accounts for the new z spectrum, resulting from a shift in ε. This

'trick' is very useful for this kind of studies because it allows to vary underlying parameters such as ε using in fact one single Monte Carlo sample, without having to undergo a time–consuming full generation every time the parameter is changed.

The value of ε_b has been taken from the fit to ALEPH data [19], which yields

$$\varepsilon_b = (4.6 \pm 0.5 \pm 0.8) \times 10^{-3}$$

while the value used in the Monte Carlo is $\varepsilon_b = 0.006$

The value of ε_c has been taken from the D^* analysis [20]:

$$\varepsilon_c = (47^{+21}_{-14} \pm 2) \times 10^{-3}$$

while the value in the Monte Carlo is $\varepsilon_c = 0.052$.

Another error comes in from the uncertainty on A_{bkg}, which is equal to the statistical error on the Monte Carlo determination of such background term.

The error on the amount of background comes from the estimates of the discrepancies between data and Monte Carlo concerning the simulation of misidentified hadrons.

We have let the relative amount of electrons and muons float by $\pm 3\%$ in order to allow for an overall uncertainty in the lepton identification efficiencies (apart from the angular and momentum dependences dealt with by the correction factors mentioned above).

The amount of events where the parent quark came from a hard gluon (which is a very small fraction) was varied by 100%.

The error caused by the uncertainty on the mixing parameter $\bar{\chi}$ turns out to be one of the most relevant contributions to the total systematic error.

The results on the contributions from the listed sources are summarized in table 11, for muons and electrons at the peak. The various contributions are added in quadrature to give an estimate on the total systematic error.

3.6 Conclusions

We have measured the forward–backward asymmetry of $Z^0 \rightarrow b\bar{b}$ events at seven energy points, and the results are listed in table 12. Fig. 17 show the measured values as a function of the centre-of-mass energy, together with the theoretical prediction by the Standard Model, for a particular value of m_{top}.

Source	Variation	$\Delta A_{\rm FB}^b(\%)$
Monte Carlo statistics	1 σ	0.04
$\Gamma(b\bar{b})/\Gamma(had)$	5%	0.09
$\chi = 0.110$	± 0.017	0.40
BR$(b \to \ell)$	1 σ	0.07
BR$(b \to c \to \ell)$	1 σ	0.05
BR$(b \to W \to \bar{c}s)$	50%	< 0.01
$(b \to W \to \bar{c}s)$ model	50%	< 0.01
BR$(b \to \tau \to \ell)$	1 σ	0.01
BR$(b \to u)$	50%	0.03
$\Gamma(c\bar{c})/\Gamma(had)\cdot$BR$(c \to \ell)$	15%	0.18
quarks from hard gluons	100 %	0.04
ε_b	1 σ	0.02
lepton ID efficiency	3%	<0.01
γ conversions	2%	<0.01
b fragmentation model		0.03
ε_c	1 σ	0.10
$A_{\rm FB}^{\rm background}$	1 σ	0.20
Bkg uncertainty	1 σ	0.03
TOTAL		0.76

Table 11: Estimated contributions of the various sources to the systematic error on $A_{FB}(b)$at the Z peak.

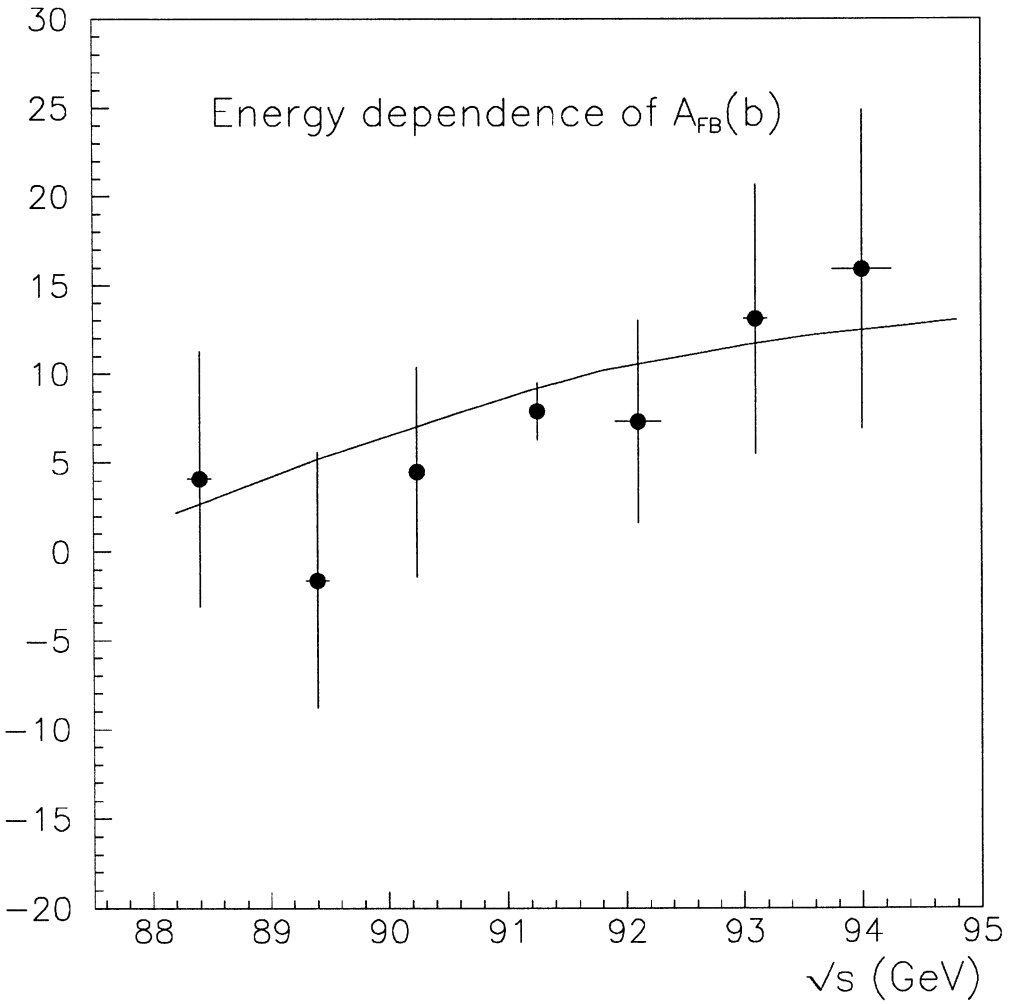

Figure 17: Extracted $A_{FB}(b)$ as a function of energy. The plotted errors are statistical only. The superimposed curve is the Standard Model prediction for $m_{top} = 130$ GeV

Energy Point	Extracted Asymmetry (%)
Peak - 3 GeV	$4.2 \pm 7.2 \pm 0.5$
Peak - 2 GeV	$-1.7 \pm 7.3 \pm 0.3$
Peak - 1 GeV	$4.5 \pm 5.9 \pm 0.5$
Peak	$7.9 \pm 1.6 \pm 0.8$
Peak +1 GeV	$7.3 \pm 5.7 \pm 0.7$
Peak +2 GeV	$13.1 \pm 7.6 \pm 1.1$
Peak + 3 GeV	$15.9 \pm 9.1 \pm 1.3$

Table 12: Values of the extracted asymmetry at seven energy points for the total sample.

P_t cut (GeV)	$A^b_{FB}(\%)$
0.75	7.8 ± 2.2
1.00	8.5 ± 1.8
1.25	7.9 ± 1.6
1.50	7.4 ± 1.7
1.75	7.9 ± 1.8
2.00	7.8 ± 2.0

Table 13: Values of the extracted asymmetry for the total sample, at various p_t cuts. The errors are statistical only.

We have also studied the stability of our result at the peak, with respect to the $p_\perp$ cut. Table 13 lists the results for 6 differents cut in $p_\perp$ (using the Altarelli model). Fig. 18 shows a plot of such values: the errors are the statistical errors on the difference between the value at a certain $p_\perp$ cut and the chosen value, which is meant to take into account the correlation of the samples at the various cuts.

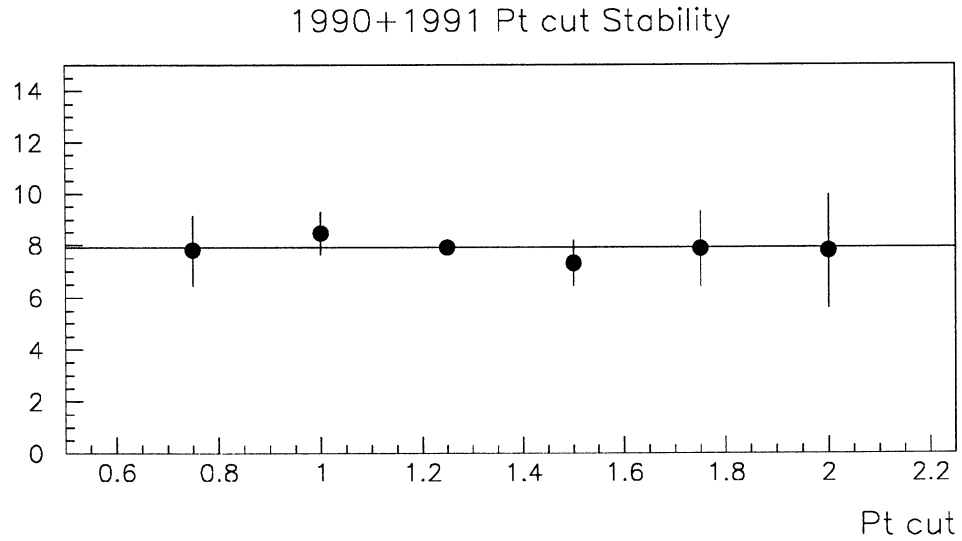

Figure 18: Extracted values of $A_{FB}(b)$ at various $p_\perp$ cuts. The errors are relative to the difference with respect to the value for the chosen cut.

4 Measuring the Mixing

Starting from the same sample we have used for the asymmetry we have selected events with two high $p_\perp$ leptons back to back, which, in most cases, will come from the decay of the two beauty hadrons. The fraction of dileptons with the same charge contains information on $B^0\bar{B}^0$ mixing. We recall that, defining χ_i as the integrated probability that the beauty hadron of type i mixes before decaying ($\chi_i = P(H_i^0 \to \bar{H}_i^0)$), we measure $\chi = f_d\chi_d + f_s\chi_s$ where f_d and f_s are the fractions of B_d^0 and B_s^0 in the beauty hadron sample (since barions and charged B mesons don't mix).

4.1 The selected sample

The lepton identification cuts have been discussed previously (section 2.5). The angle between the two leptons has to be greater than 90 degrees, to select leptons coming from hadrons in opposite hemispheres. The leptons in the event are ordered according to their $p_\perp$; if the first lepton and the second

one are on the same side, the first and the third are considered, and so on, till a pair which fulfils all the conditions is found, or there are no more leptons in the event. In extracting the mixing, we have to take into account all the possible combinations, on the two sides, of the following channels:

$$
\begin{array}{l}
b \to \ell \\
b \to \tau \to \ell \\
b \to c \to \ell \\
b \to W \to \bar{c} \to \ell \\
c \to \ell \\
fake
\end{array}
$$

It's easily seen that the $b \to c \to \ell$ component gives the wrong information about the quark charge, and therefore, when it's coupled with one of the other channels with a lepton coming from a b quark, it gives a background which tends to cancel the signal.

The $c \to \ell$ component can only be coupled with itself, giving opposite charge dileptons, or, less frequently, with a *fake* lepton.

The *fake* component can be coupled with all the others; the main contribution is $(b \to \ell)$ (*fake*). This component does not give exactly 50% same charge and 50% opposite charge dileptons, since even in *fakes* some memory of the original quark charge is kept. This is due to the fact that also the misidentified particle fulfils the kinematic cuts. We will try to measure from data the fraction of these pairs which has the same charge.

Our method is to select a pure sample of $(b \to \ell)$ $(b \to \ell)$ through a $p_\perp$ cut, then to count the number of same charge, opposite side lepton pairs in data, and finally to extract the value of mixing taking the composition of the sample from Monte Carlo [10].

We remark here that we cannot be sure that the beauty–hadron mixture is exactly the same for $b \to \ell$ and $b \to c \to \ell$. In fact the selection is based on leptons; since the semileptonic branching ratios of charmed hadrons are different, in $b \to c \to \ell$ we *prefer* certain kinds of charmed hadrons, and therefore certain kinds of *beauty* hadrons. So f_d and f_s could be different for

[10] In addition to the Monte Carlo with standard mixture of flavours, we have largely used here $b\bar{b}$ MC events, which help to evaluate the relative abundancies of classes in which there is a lepton coming from a b, which, in total, represent about 99% of the sample at the chosen cut.

$b \to \ell$ and $b \to c \to \ell$, and therefore could be different χ. However this effect is negligible at the present level of statistical precision [17].

4.2 The background charge correlation

We have measured the background charge correlation from data, requiring two tracks in opposite hemispheres which fulfil the kinematic cuts, asking no lepton identification. With the selected pairs we have computed

$$\xi = \left.\frac{N_{same\ charge}}{N_{pairs}}\right|_{background} = 0.48 \pm 0.01$$

In order to check if there is some systematic effect on this number, we have tried to remove the requirement of no lepton identification, and to introduce some very loose cuts on the variables used in lepton identification (to select *lepton-like* tracks). The parameter ξ is found to be quite stable with respect to these selection criteria. Also the $p_\perp$ dependence, in the range considered, is found to be negligible.

4.3 The mixing from high $p_\perp$ leptons

We now proceed counting the same charge and opposite charge pairs in data and extracting the value of mixing. In doing this we have in mind that

- pairs with both leptons coming from a b quark contribute to the fraction of same charge dileptons with $2\chi(1-\chi)$ if both leptons have the right or the wrong information about the quark charge; they contribute with $\chi^2 + (1-\chi)^2$ if one has the right information and the other the wrong one
- pairs with both leptons from a c quark give no contribution to the fraction of same charge dileptons
- pairs with a *fake* lepton contribute to the fraction of same charge dileptons with ξ (see above).

Correction factors have been applied to the Monte Carlo in order to use the b semileptonic branching ratios (table 10) which are obtained fitting the ALEPH data [19] with the Altarelli model for the b decay, which is the one

used in our Monte Carlo. Later on we will investigate the dependence of our measurement on the decay model assumed for the b quark.

We have also applied correction factors to take into account the small known discrepancies in the simulation of electron and muon efficiencies and of their background [11]; these correction factors have, however, a tiny effect on the final result.

We have performed the calculation for different $p_\perp$ cuts, in order to choose the cut which allows the most precise measurement, and we have explored a large range as a check of our understanding of systematics.

In figg. 19 and 20 are shown the momentum and transverse momentum spectra of the selected leptons in data and Monte Carlo. The plots are normalized to the same number of entries (since we don't care about absolute efficiencies) and show that the simulation fits data very well. In tables 14 and 15, the Monte Carlo sample fractional compositions are quoted for different cuts (we show only the most *crowded* classes, and put together the others); in tables 16, 17 the numbers of pairs and of same charge pairs selected in data and the resulting mixing values with the statistical error are shown.

Defining

$$R = \left. \frac{N_{same\ charge}}{N_{pairs}} \right|_{data}$$

we have that the statistical error on the mixing is given by the statistical error on R, which is larger for hard cuts, increased by the factor which links R to χ, which is smaller for high purities, *i.e.* for hard cuts. Therefore the statistical error has a minimum in the region between $p_\perp > 1$ and $p_\perp > 1.25$ GeV/c. The highest of the two cuts is chosen since the higher is the purity, the lower is the systematic error.

The results with all the statistics (1990 + 1991) are shown in table 20.

We are now interested in seeing if the discrepancies between different measurements are compatible with being statistical fluctuations. In order to do that we have to take into account the fact that each sample includes all the samples obtained with harder cuts, so that each value is correlated with all the others. We keep the value obtained with the chosen cut as the reference point, and calculate the errors on the difference between the other

[11] For muon efficiency see section 2.2. For muon background see appendix A

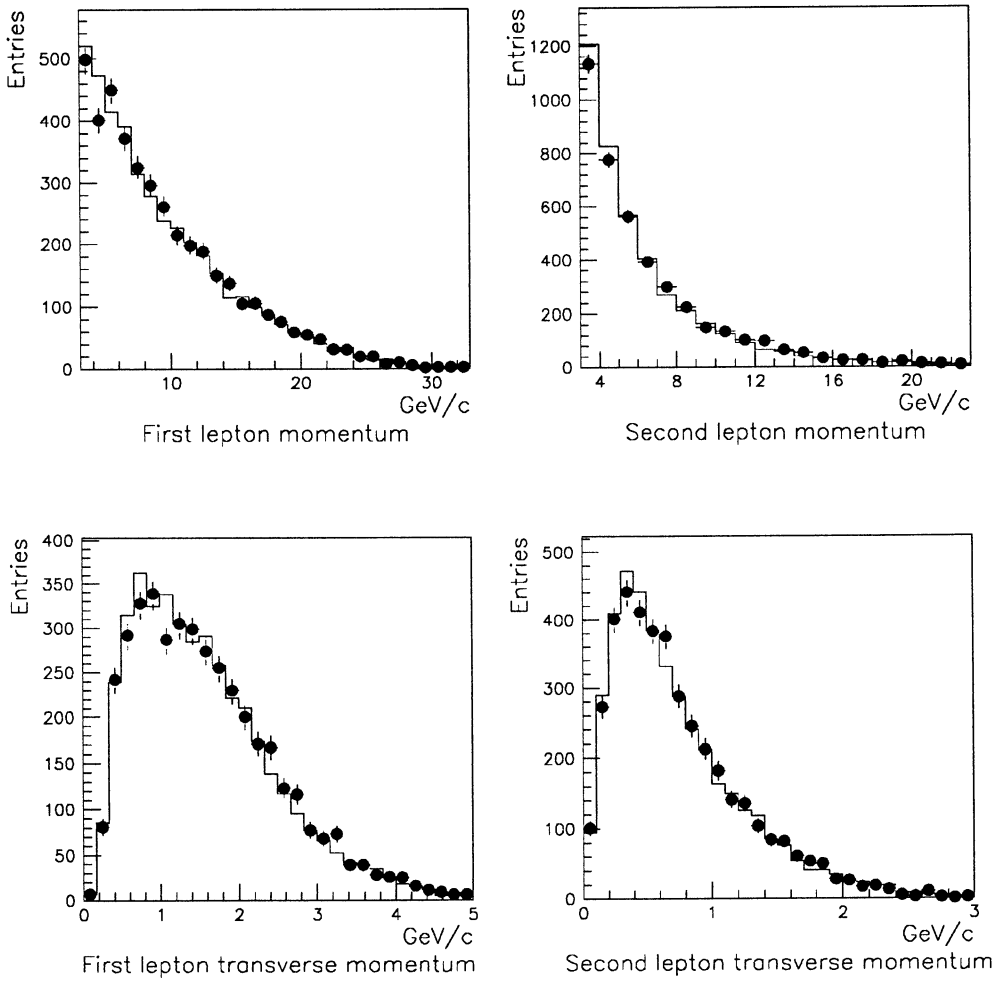

Figure 19: Momentum and transverse momentum spectra of the selected leptons in 1991 data (dots) and Monte Carlo (histogram).

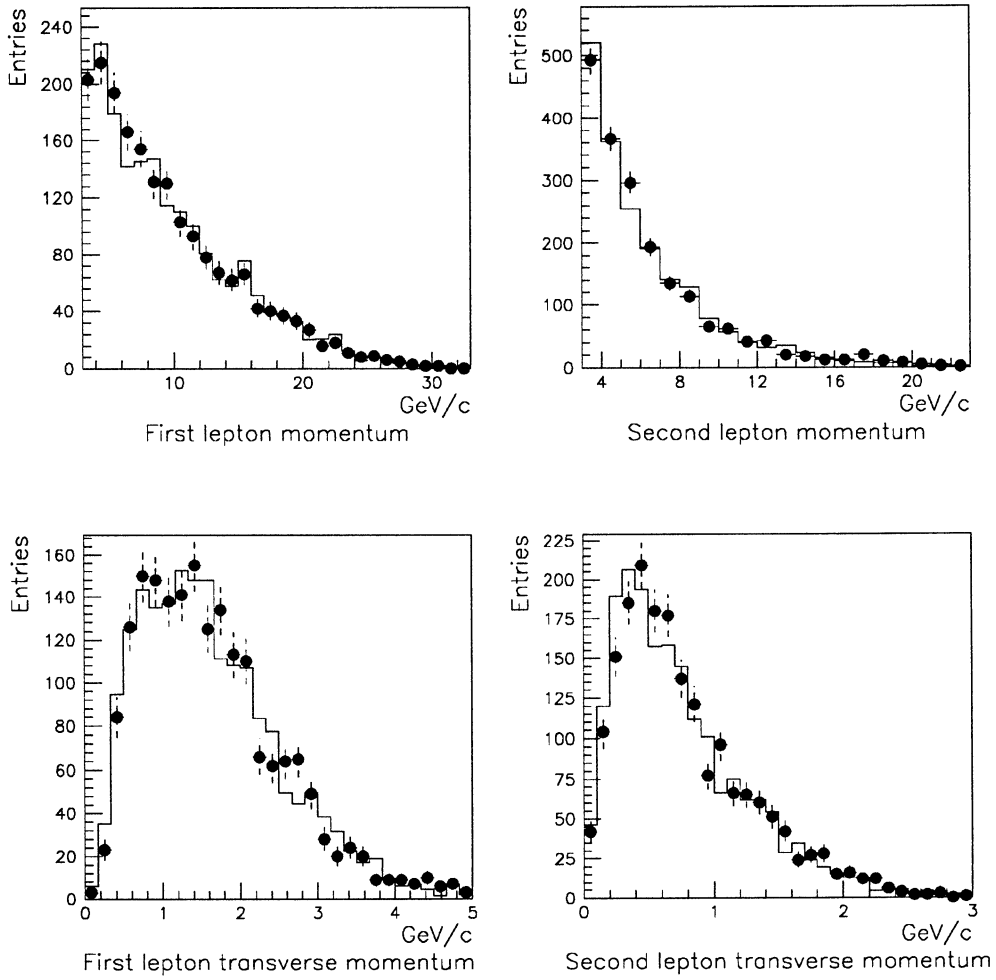

Figure 20: Momentum and transverse momentum spectra of the selected leptons in 1990 data (dots) and Monte Carlo (histogram).

$p_\perp$cut	Monte Carlo composition: dileptons from b				
	$b \to \ell$	$b \to \ell$	$b \to \ell$	$b \to \ell$	$b \to X \to \ell$
	$b \to \ell$	$b \to \tau \to \ell$	$b \to c \to \ell$	$b \to \bar{c} \to \ell$	$b \to X \to \ell$
0.75	55.1±1.3	2.7±0.4	20.1±1.0	1.7±0.3	3.5±0.5
1.00	66.2±1.5	1.9±0.4	17.1±1.2	1.1±0.3	2.2±0.5
1.25	74.9±1.7	1.9±0.5	13.6±1.4	0.6±0.3	0.6±0.3
1.50	79.7±2.1	1.0±0.5	11.4±1.7	0.3±0.3	0.3±0.3
1.75	82.2±2.6	1.4±0.8	9.2±2.0	0.5±0.5	0.5±0.5
2.00	83.5±3.4	1.6±1.2	7.7±2.4	0.8±0.8	< 0.8

$p_\perp$cut	Monte Carlo composition: other channels			
	$c \to \ell$	$b \to \ell$	$b \to X \to \ell$	X
	$c \to \ell$	*fake*	*fake*	X
0.75	1.9±0.5	9.0±0.7	2.4±0.4	3.1±0.6
1.00	0.7±0.4	8.2±0.9	1.3±0.4	1.9±0.6
1.25	0.3±0.3	7.1±1.0	0.8±0.4	0.4±0.3
1.50	< 0.4	6.7±1.3	0.7±0.4	< 0.4
1.75	< 0.5	6.3±1.7	< 0.5	< 0.5
2.00	< 0.8	6.4±2.2	< 0.8	< 0.8

Table 14: Monte Carlo composition for various cuts. 1990 sample, Altarelli model.

$p_\perp$cut	Monte Carlo composition: dileptons from b				
	$b \to \ell$	$b \to \ell$	$b \to \ell$	$b \to \ell$	$b \to X \to \ell$
	$b \to \ell$	$b \to \tau \to \ell$	$b \to c \to \ell$	$b \to \bar{c} \to \ell$	$b \to X \to \ell$
0.75	56.4±0.8	2.6±0.3	19.0±0.6	2.0±0.2	3.3±0.3
1.00	67.9±0.9	2.1±0.3	15.5±0.7	1.3±0.2	1.8±0.3
1.25	76.0±1.1	1.8±0.3	12.2±0.8	0.7±0.2	0.8±0.2
1.50	81.7±1.2	1.7±0.4	9.2±0.9	0.4±0.2	0.3±0.2
1.75	84.8±1.5	1.7±0.5	7.5±1.1	0.2±0.2	< 0.2
2.00	88.0±1.7	1.9±0.7	5.7±1.2	0.3±0.3	< 0.3

$p_\perp$cut	Monte Carlo composition: other channels			
	$c \to \ell$	$b \to \ell$	$b \to X \to \ell$	X
	$c \to \ell$	*fake*	*fake*	X
0.75	2.2±0.3	8.9±0.5	2.1±0.2	3.3±0.3
1.00	1.5±0.3	7.4±0.5	1.2±0.2	2.0±0.3
1.25	0.7±0.2	6.3±0.6	0.8±0.2	0.9±0.3
1.50	0.3±0.2	5.2±0.7	0.4±0.2	0.9±0.4
1.75	< 0.2	4.2±0.8	0.3±0.3	1.4±0.6
2.00	< 0.3	3.6±1.0	< 0.3	0.4±0.4

Table 15: Monte Carlo composition for various cuts. 1991 sample, Altarelli model.

$p_\perp$ cut	Lepton pairs		Mixing value
	selected pairs	same charge pairs	$\chi \pm \Delta\chi$ (stat.)
0.75	574	197	0.109 ± 0.027
1.0	400	118	0.085 ± 0.023
1.25	255	72	0.105 ± 0.026
1.5	157	43	0.111 ± 0.031
1.75	100	27	0.118 ± 0.037
2.0	51	14	0.127 ± 0.052

Table 16: Lepton pairs in data and extracted mixing value for various cuts. 1990 sample.

$p_\perp$ cut	Lepton pairs		Mixing value
	selected pairs	same charge pairs	$\chi \pm \Delta\chi$ (stat.)
0.75	1179	417	0.132 ± 0.019
1.0	766	241	0.119 ± 0.018
1.25	495	140	0.112 ± 0.018
1.5	304	77	0.103 ± 0.020
1.75	174	37	0.081 ± 0.023
2.0	91	22	0.114 ± 0.034

Table 17: Lepton pairs in data and extracted mixing value for various cuts. 1991 sample.

points and that one, taking into account the correlation. What comes out is plotted in fig. 21, which shows the good stability of our measurement.

4.4 The b decay model

In order to study to which extent our result is dependent on the decay model assumed for the b quark, we have applied correction factors to our Monte Carlo in order to use the ISGW model.

In this case we have used for the b semileptonic branching ratios the values fitted from ALEPH data [19] using this softer spectrum for the semileptonic b decay (see table 10). We have calculated again the sample compositions for different cuts, which are shown in tables 18 and 19.

A comparison between the $b \to \ell$ and $b \to c \to \ell$ spectra predicted by the two models (with the normalization given by the different branching ratios from the ALEPH fit) is presented in fig. 22.

We show in table 20 the comparison of the results obtained with the two models, using the full statistics (1990 + 1991). It can be easily seen that the difference between the two models goes down at high $p_\perp$.

The stability plots of our mixing measurement using ISGW model are shown in fig. 23.

4.5 The systematic errors

Almost all sources of systematic errors for the mixing measurement are the same as in the asymmetry case.

In particular for the mixing it holds *a fortiori* that the effects related to the acceptance have little influence, since no angular or momentum distribution is involved. Therefore we concentrate on the effects of the uncertainty in the underlying physical parameters of the Monte Carlo.

The procedures for the calculation are exactly the same as for the asymmetry. We remark that with the dilepton sample the charm component is almost absent, therefore the largest systematics come from the parameters affecting the relative abundancies of the different $b \to X$ channels.

The only systematic error which is included here and not in the case of the asymmetry is the uncertainty in the background charge correlation, whose measurement has been described previously.

The results are shown in table 21.

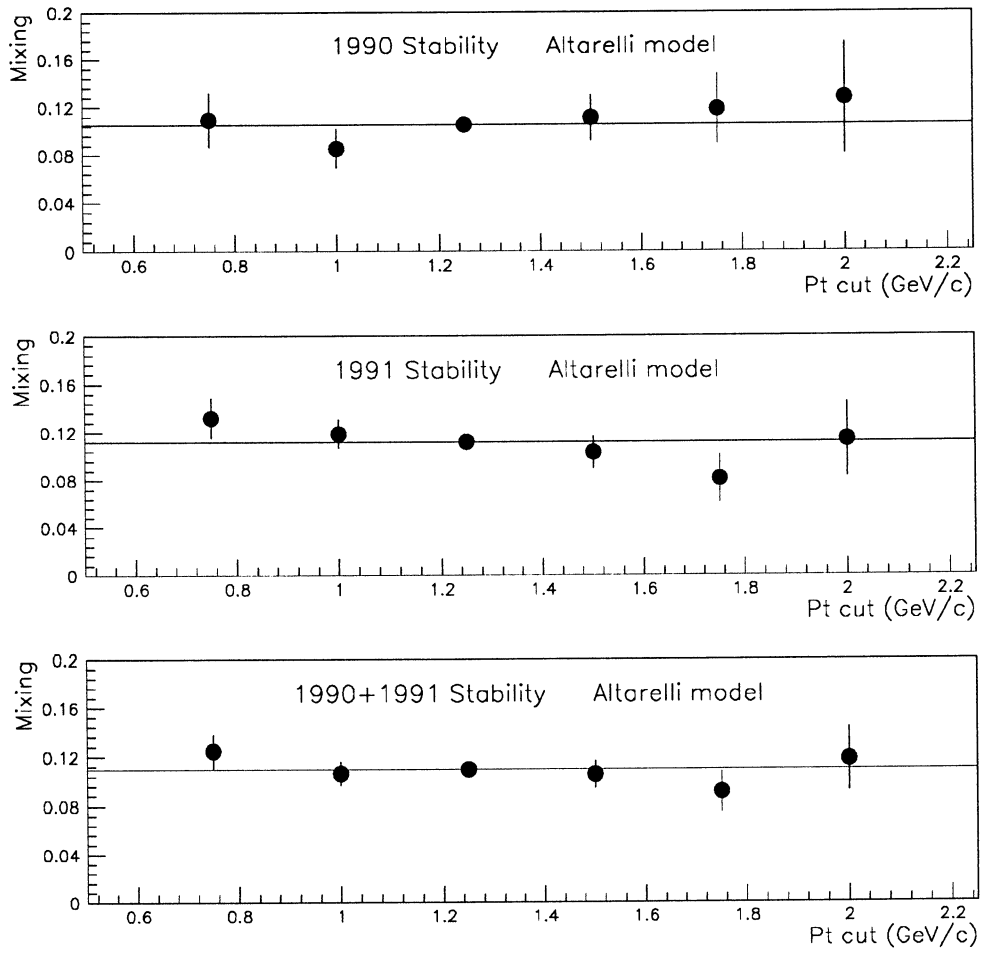

Figure 21: Stability of mixing measurement with respect to changing the $p_\perp$ cut.

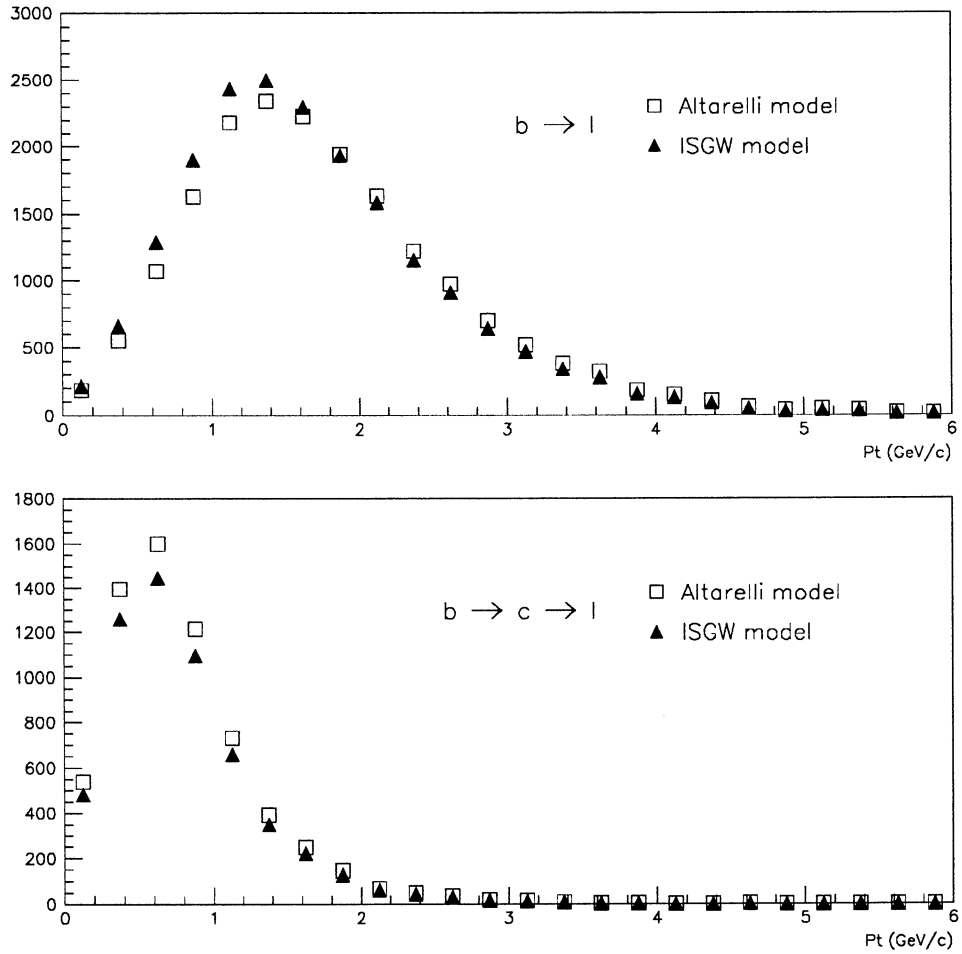

Figure 22: Comparison between $b \to \ell$ and $b \to c \to \ell$ spectra predicted by Altarelli and ISGW models.

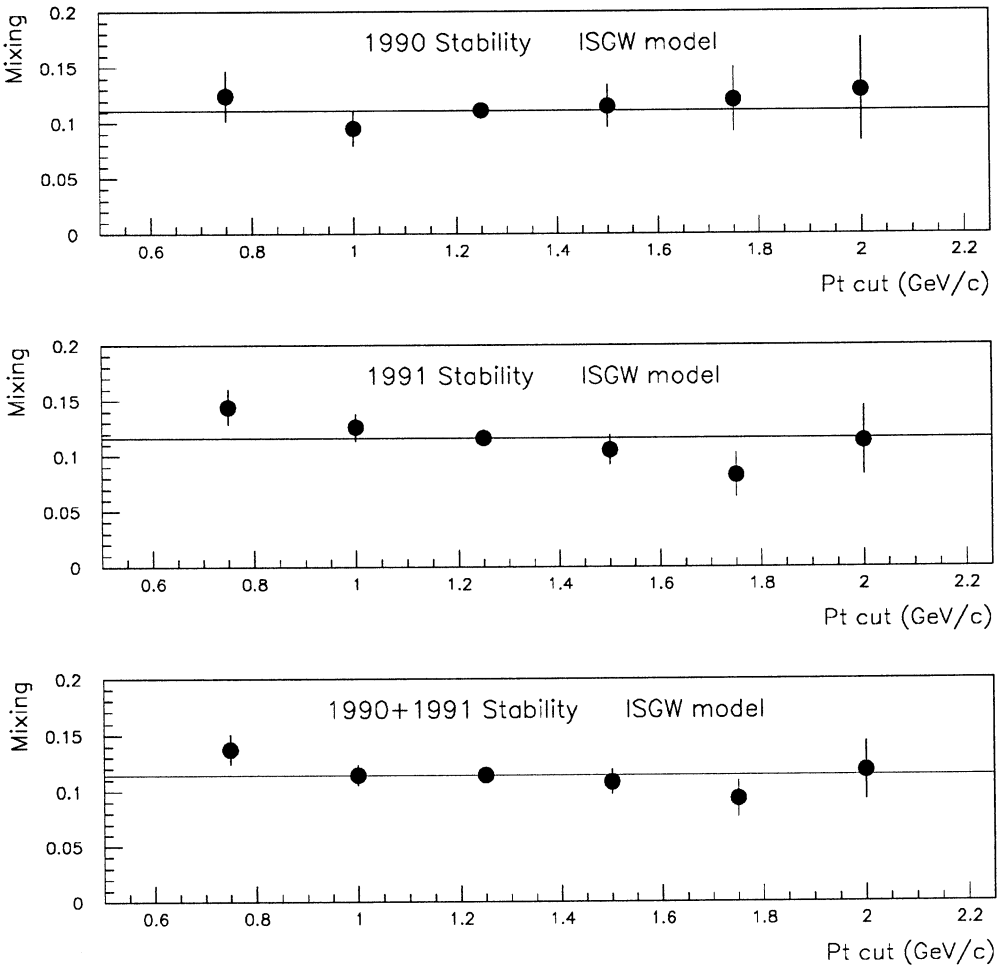

Figure 23: Stability plots using ISGW model.

$p_\perp$cut	Monte Carlo composition: dileptons from b				
	$b \to \ell$	$b \to \ell$	$b \to \ell$	$b \to \ell$	$b \to X \to \ell$
	$b \to \ell$	$b \to \tau \to \ell$	$b \to c \to \ell$	$b \to \bar{c} \to \ell$	$b \to X \to \ell$
0.75	56.5±1.3	2.8±0.4	19.0±1.0	1.8±0.3	3.1±0.5
1.00	67.2±1.5	2.0±0.5	16.1±1.2	1.1±0.3	2.1±0.5
1.25	75.5±1.8	2.2±0.6	12.8±1.4	0.6±0.3	0.6±0.3
1.50	80.0±2.2	1.2±0.6	10.9±1.7	0.2±0.2	0.3±0.3
1.75	82.1±2.8	1.7±0.9	8.9±2.1	0.4±0.4	0.5±0.5
2.00	83.0±3.7	2.2±1.4	7.2±2.6	0.8±0.8	< 0.8

$p_\perp$cut	Monte Carlo composition: other channels			
	$c \to \ell$	$b \to \ell$	$b \to X \to \ell$	X
	$c \to \ell$	*fake*	*fake*	X
0.75	1.6±0.5	9.0±0.7	2.3±0.4	3.0±0.6
1.00	0.7±0.4	8.3±0.9	1.3±0.4	1.9±0.6
1.25	0.3±0.3	7.2±1.1	0.8±0.4	0.4±0.4
1.50	< 0.3	6.8±1.4	0.7±0.5	< 0.3
1.75	< 0.5	6.4±1.8	< 0.5	< 0.5
2.00	< 0.8	6.8±2.5	< 0.8	< 0.8

Table 18: Monte Carlo composition for various cuts. 1990 sample, ISGW model.

$p_\perp$cut	Monte Carlo composition: dileptons from b				
	$b \to \ell$	$b \to \ell$	$b \to \ell$	$b \to \ell$	$b \to X \to \ell$
	$b \to \ell$	$b \to \tau \to \ell$	$b \to c \to \ell$	$b \to \bar{c} \to \ell$	$b \to X \to \ell$
0.75	57.6±0.8	2.6±0.3	18.0±0.6	2.0±0.2	3.0±0.3
1.00	68.6±0.9	2.1±0.3	14.6±0.7	1.3±0.2	1.6±0.3
1.25	76.1±1.1	1.9±0.3	11.7±0.8	0.7±0.2	0.7±0.2
1.50	81.4±1.3	1.9±0.5	8.9±0.9	0.5±0.2	0.3±0.2
1.75	84.4±1.6	1.9±0.6	7.3±1.1	0.2±0.2	< 0.3
2.00	86.9±2.0	2.3±0.9	5.8±1.4	0.4±0.3	< 0.4

$p_\perp$cut	Monte Carlo composition: other channels			
	$c \to \ell$	$b \to \ell$	$b \to X \to \ell$	X
	$c \to \ell$	*fake*	*fake*	X
0.75	1.9±0.3	9.1±0.5	2.0±0.2	3.3±0.3
1.00	1.3±0.3	7.6±0.5	1.2±0.2	2.0±0.3
1.25	0.6±0.2	6.6±0.6	0.8±0.2	0.9±0.3
1.50	0.3±0.2	5.5±0.8	0.4±0.2	1.0±0.4
1.75	< 0.3	4.4±0.9	0.3±0.3	1.5±0.6
2.00	< 0.4	4.2±1.2	< 0.4	0.4±0.4

Table 19: Monte Carlo composition for various cuts. 1991 sample, ISGW model.

$p_\perp$cut	Mixing with statistical error	
	Altarelli model	ISGW model
0.75	0.125 ± 0.016	0.137 ± 0.015
1.00	0.106 ± 0.014	0.114 ± 0.014
1.25	0.110 ± 0.015	0.114 ± 0.015
1.50	0.105 ± 0.017	0.108 ± 0.017
1.75	0.091 ± 0.019	0.093 ± 0.019
2.00	0.118 ± 0.028	0.118 ± 0.028

Table 20: Comparison between Altarelli and ISGW decay model with full statistics.

4.6 The different lepton channels

We have tried to evaluate mixing using separately the two kind of leptons, and the combinations of an electron on one side and a muon on the other, in order to check whether any systematics related to the lepton identification could be found.

The results are summarized in table 22 for different $p_\perp$ cuts. We don't further divide the samples into the two years of data taking in order to have reasonable statistics.

For each cut the three results are obtained from completely independent data and Monte Carlo samples, so they can be simply compared taking into account the statistical error. No clear discrepancy is found.

Again we are interested in seeing if some systematic effects related with the $p_\perp$ cut can be put into evidence, for any of the three different subsamples. With the procedure described in section 4.4 we get the plots of fig. 24,which show the good stability of each measurement.

In order to get more informations about the stability of our measurement with respect to changing the $p_\perp$ cut or the lepton sample used, we can compare in one plot the *final* mixing value obtained with the full statistics and the cut $p_\perp > 1.25$, with the values computed with different $p_\perp$ cuts and different lepton subsamples. Again, we use the errors on the difference between the considered value and the value obtained with the full statistic and the chosen cut, taking into account the correlation between the two measurements. The

Source	Variation	$\Delta\chi$
Monte Carlo statistics	1 σ	0.0052
$\Gamma(b\bar{b})/\Gamma(had)$	5 %	< 0.0001
BR($b \rightarrow \ell$)	1 σ	0.0022
BR($b \rightarrow c \rightarrow \ell$)	1 σ	0.0053
BR($b \rightarrow W \rightarrow \bar{c} \rightarrow \ell$)	50 %	0.0002
$b \rightarrow W \rightarrow \bar{c} \rightarrow \ell$ model	50 %	0.0002
$\Gamma(c\bar{c})/\Gamma(had)$*BR($c \rightarrow \ell$)	15 %	0.0001
BR($b \rightarrow \tau \rightarrow \ell$)	1 σ	0.0002
lepton ID efficiency	3 %	< 0.0001
ε_b	1 σ	0.0001
ε_c	1 σ	< 0.0001
b fragmentation	2 models	0.0002
γ conversions	2 %	< 0.0001
electron background	10 %	< 0.0001
muon background	20 %	0.0005
quarks from hard gluons	100 %	0.0007
BR($b \rightarrow u$)	50 %	0.0009
Background charge correlation	1 σ	0.0006
TOTAL		0.0078

Table 21: Estimated contributions of the various sources to the systematic error on χ.

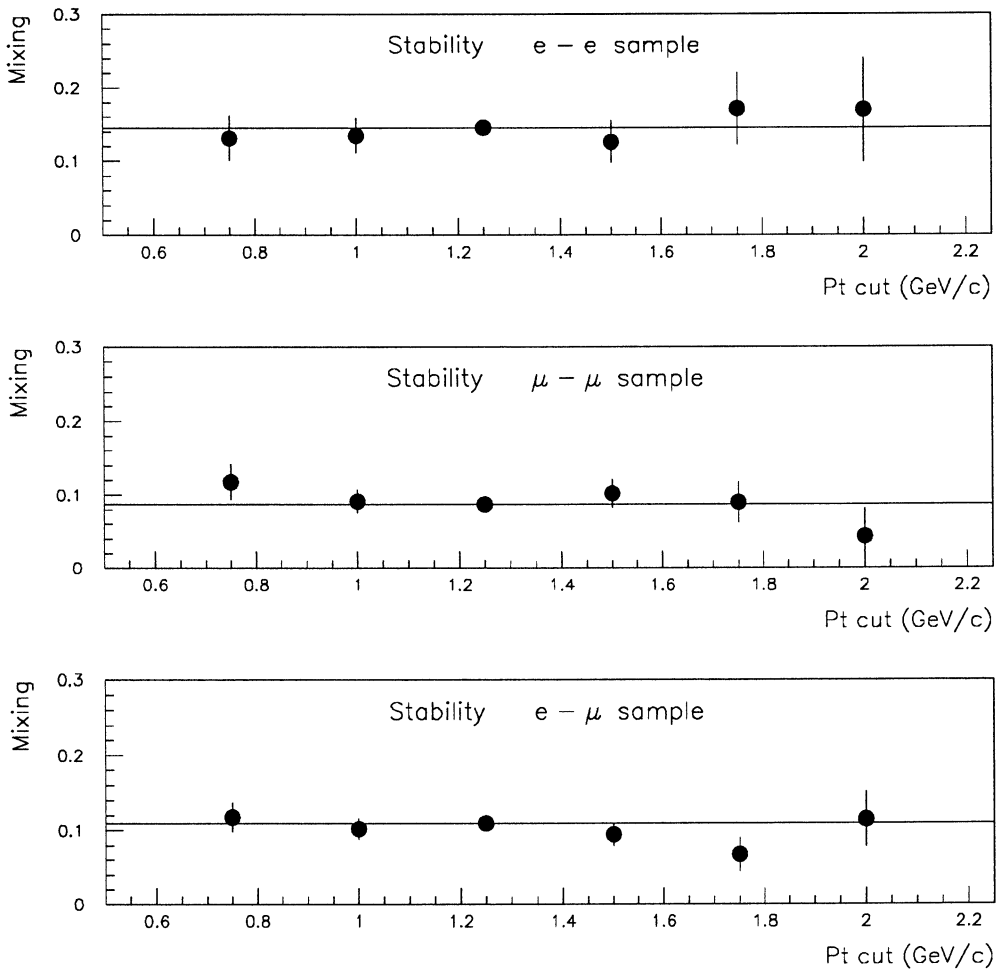

Figure 24: Stabiltity plots for the three different subsamples.

result of this study is shown in fig. 25. The measurement seems to be very robust, since almost all the values are within one sigma from the *final* value. The fact that, for instance, all the values from electrons are above the line indicating the *final* value is not so surprising since they are all correlated, so we expect that if a fluctuation occurs in the electron subsample, it will influence the measurement at different $p_\perp$ cuts.

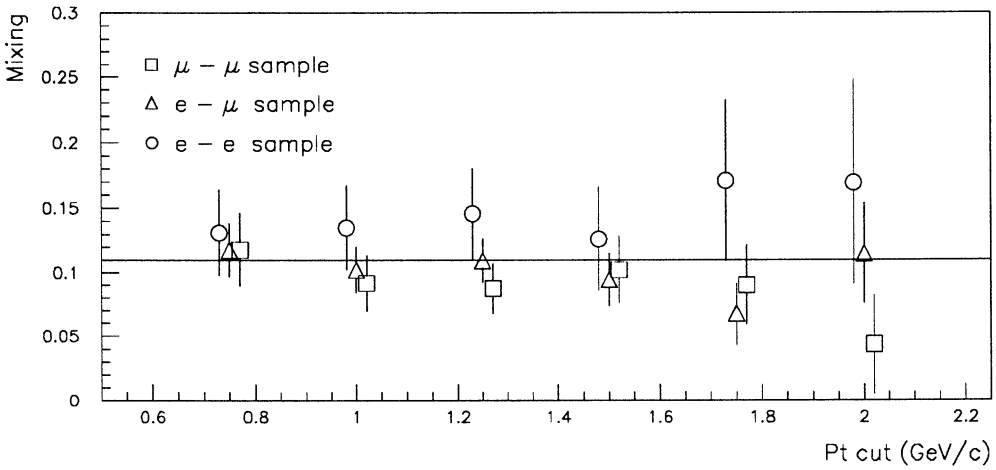

Figure 25: Compatibility of measurements obtained with different subsamples and different $p_\perp$ cuts. The dots corresponding to the e–e and to the μ–μ samples are a little bit shifted from the correct value of the $p_\perp$ cut in order to make the plot easier to be read.

4.7 Mixing and asymmetry using CLEO results

As can be seen from table 10, the values of the BR($b \to \ell$) and BR($b \to c \to \ell$) obtained from the fit of the ALEPH spectra [19] are rather different from the Monte Carlo values based on the CLEO spectra within the Altarelli model.

If we repeat our asymmetry and mixing measurements using the latest values from CLEO [28], we get the results shown in table 23.

$p_\perp$ cut	Mixing with statistical error		
	e – e	μ – μ	e – μ
0.75	0.131 ± 0.034	0.118 ± 0.030	0.118 ± 0.022
1.00	0.135 ± 0.034	0.092 ± 0.025	0.102 ± 0.021
1.25	0.146 ± 0.038	0.088 ± 0.025	0.110 ± 0.023
1.50	0.126 ± 0.042	0.103 ± 0.029	0.094 ± 0.025
1.75	0.171 ± 0.063	0.090 ± 0.032	0.067 ± 0.027
2.00	0.169 ± 0.080	0.043 ± 0.039	0.115 ± 0.043

Table 22: Comparison between different lepton channels with full statistics.

	Altarelli model	ISGW model
Asymmetry	0.080 ± 0.016 ± 0.008	0.080 ± 0.017 ± 0.008
Mixing	0.099 ± 0.015 ± 0.009	0.100 ± 0.015 ± 0.009

Table 23: Asymmetry and mixing using CLEO branching ratios.

4.8 Conclusions

In conclusion our analysis of the dilepton sample gives

$$\chi = 0.112 \pm 0.015(stat.) \pm 0.008(syst.) \pm 0.002(model)$$

A Muon background

Pion contamination is the dominant source of background to muons identified in hadronic events. A pion can fake a muon in the HCAL basically in three ways: by decaying semileptonically to a muon, by not interacting in the calorimeter (sail–through) and by showing an interaction pattern recognized as a muon by the muon identification algorithm (this can occur easily when one of the secondaries decays to a muon whose track lies in the multiple scattering cone of the primary hadron). We will try to check if this background is well simulated by our Monte Carlo selecting pure samples of hadrons without using HCAL information in suitable physical channels, and performing on them the standard muon identification cuts.

In single–prong τ decays it is possible to select a very pure sample of pions, using the $\rho^{\pm}$ channel, as is done in [14]. This yields a very simple and clean analysis; the limitation of this method is the statistics of the sample.

Another useful channel is three–prong τ decays (see [15]). In this case we also get a pure sample of hadrons, after having carefully rejected single–prong decays with a photon converting into an electron pair, which simulate the three–prong pattern.

To get a good statistics it is necessary to use hadronic events. The obvious channel is K^0 decaying to $\pi^+\pi^-$ (see [15]), which is however not as clean as the previous ones.

Since we aim to study the behaviour of hadronic showers we have avoided geometrical effects by restricting our search to the Barrel ($|\cos\theta| < 0.6$). We have performed these studies on 1991 data and Monte Carlo, (Galeph version 250 for $\tau^+\tau^-$ events, versions 242, 250, 251 for $q\bar{q}$ events; Julia version 258) on 1990 data and the new version of 1990 Monte Carlo (Galeph version 252, which uses Geant 3.15, Julia version 260).

Particle ID	Number	Fraction (%)
Mismatch	3	0.04 ± 0.03
$\tau \rightarrow e$	31	0.46 ± 0.08
$Had. \rightarrow \mu$	19	0.28 ± 0.06
Hadrons	6734	99.22 ± 0.11
Total	6787	

Table 24: Composition of the one–prong sample from 1991 Monte Carlo.

A.1 Event selection

The selection of $\tau^+\tau^-$ events is done with the programme SELTAU [16] which gives an efficiency of about 75 %. Our Monte Carlo samples are composed of 50000 $\tau^+\tau^-$ events in both years of which SELTAU accepts respectively 36089 in 1991, and 36519 in 1990. In data we starts with class 15 events (leptons) which fulfil EW group data quality requirements, respectively 64356 in 1991 and 34277 in 1990, of which SELTAU recognises as $\tau^+\tau^-$ 10770 and 5609.

For the single–prong channel, we search for $\rho^{\pm}$ decays in the following way. The event is divided into two hemispheres using the thrust axis, and charged tracks that are isolated within their hemisphere are retained. In order to reject τ decays to electrons and muons, we tag events with a reconstructed π^0 in the ECAL. This is basically a $\rho^{\pm}$ sample, even if we do not perform any cut on the large ρ resonance. Photons (taken from EGPC bank) which lie in a cone of 37 degrees around the track are selected and paired in order to calculate the pair invariant mass. We choose the pair which has the invariant mass M_{12} closest to the π^0 mass and we select events with $0.05 < M_{12} < 0.2$ GeV/c^2.

This yields a very high purity hadron sample. In the barrel we select 1925 and 6787 tracks with $P > 3$GeV/c in 1991 data and Monte Carlo respectively, 1141 and 7072 in 1990. In tables 24 and 25 the compositions estimated from Monte Carlo for 1991 and 1990 samples respectively are shown, where we have flagged as *mismatch* the tracks in which the association of the reconstructed track to the generated particle was not successful. The class *decays* contains only μ from hadrons which decay within the TPC volume: this is is done because in this way the amount of *decays* depends basically only on the

Particle ID	Number	Fraction (%)
Mismatch	3	0.04 ± 0.02
$\tau \rightarrow e$	30	0.42 ± 0.08
$Had. \rightarrow \mu$	20	0.28 ± 0.06
Hadrons	7019	99.24 ± 0.10
Total	7072	

Table 25: Composition of the one–prong sample from 1990 Monte Carlo.

hadron lifetime (since the amount of material inside the TPC volume is very small), while the rate of decays in the calorimeters depends also on the simulation of the material, and is therefore less reliable. No $\tau \rightarrow \mu$ decay is selected. The probability that a track coming from a $\mu^+\mu^-$ contaminates our sample has been computed with the Monte Carlo and it is totally negligible (of the order of 10^{-6}).

For the three–prong τ decays, we require 3 good charged tracks in the hemisphere, with a momentum greater than 1.5 GeV/c. This selects τ decays into three charged pions, with a few percent contamination of one–prong events with a photon converting in an e^+e^- pair, which simulates a three–prong pattern. In order to reduce this contamination we require that none of the three tracks be identified as an electron (according to the standard electron identification described in section 2.3), and that none of the pairs built with the three tracks be compatible with being a photon conversion. In this way we select respectively 2497 and 8309 tracks in 1991 data and Monte Carlo, 1244 and 8838 in 1990. In tables 26 and 27 are shown respectively the composition of 1991 and 1990 Monte Carlo samples found with this selection. Neither muons nor electrons from direct τ decay are selected.

For the K^0 decays in hadronic events, we start by requiring the standard hadronic event selection 2.1. Then we use V^0s from the YV0V bank, asking the V^0 to be a *good* particle, with the same cuts as for charged particles, with additional requirements $P(V^0) > 2$ GeV/c and $\chi^2(V^0) < 6$. The V^0 has to be compatible with the K^0 mass hypotesis (within 10 MeV) and not with the γ and Λ^0. Even if the V^0 algorithm works efficiently, we get in this way some prompt muons in the combinatorial background: they are a small fraction of the initial sample, but become important when we apply the

Particle ID	Number	Fraction (%)
Mismatch	4	0.05 ± 0.02
$\gamma \rightarrow e^+e^-$	45	0.54 ± 0.08
$Had. \rightarrow \mu$	36	0.43 ± 0.07
Hadrons	8224	98.98 ± 0.11
Total	8309	

Table 26: Composition of the three–prong sample from 1991 Monte Carlo.

Particle ID	Number	Fraction (%)
Mismatch	4	0.05 ± 0.02
$\gamma \rightarrow e^+e^-$	36	0.41 ± 0.07
$Had. \rightarrow \mu$	31	0.35 ± 0.06
Hadrons	8767	99.20 ± 0.09
Total	8838	

Table 27: Composition of the three–prong sample from 1990 Monte Carlo.

muon identification cuts (see tables 28 and 29). As these prompt muons are mainly in heavy flavour events, we lower the fraction of heavy flavour events in our sample using their property to lose, on average, more energy through neutrinos. If we cut on the top of the peak of the Energy Flow reconstructed energy, keeping only the events on the right of the peak, we fairly reduce this contamination, even if we lose about half statistics. (We remark here that the Energy Flow peak is shifted in Monte Carlo with respect to data, so our cuts will be $E > 90.54$ GeV for data, $E > 91.63$ GeV for 1991 Monte Carlo, $E > 91.96$ GeV for 1990 Monte Carlo). The Monte Carlo compositions for various cuts are listed in table 28 for 1991 and table 29 for 1990. The analysis is done with the cut on the reconstructed energy. Selected tracks are 12402 in data and 30023 in Monte Carlo 1991, 6415 in data and 9950 in Monte Carlo 1990.

A.2 Results

With the samples selected we have checked the behaviour of HCAL with respect to the variables commonly used to reject hadrons.

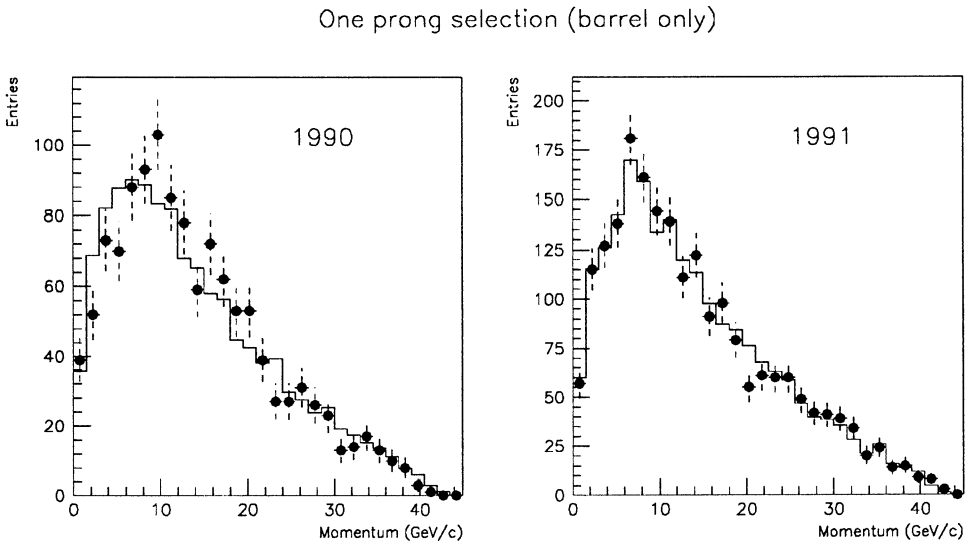

Figure 26: Momentum spectra of the selected tracks in data (dots) and Monte Carlo (histogram).

		Cuts		
		none	11.*or*.13.*or*.14	13.*or*.14
Mismatch	n	16	0	0
	%	0.03 ± 0.01	0	0
Electrons	n	688	0	0
	%	1.18 ± 0.04	0	0
Prompt μ	n	123	112	109
	%	0.21 ± 0.02	17.9 ± 1.5	23.9 ± 2.0
$Had. \rightarrow \mu$	n	245	160	147
	%	0.42 ± 0.03	25.6 ± 1.7	32.2 ± 2.2
Hadrons	n	57088	352	200
	%	98.16 ± 0.06	56.4 ± 2.0	43.9 ± 2.3
Total		58160	624	456

		Cuts		
		E ≥ 91.63	E ≥ 91.63 11.*or*.13.*or*.14	E ≥ 91.63 13.*or*.14
Mismatch	n	12	0	0
	%	0.04 ± 0.01	0	0
Electrons	n	329	0	0
	%	1.10 ± 0.06	0	0
Prompt μ	n	31	27	26
	%	0.10 ± 0.02	9.3 ± 1.7	12.7 ± 2.3
$Had. \rightarrow \mu$	n	126	82	75
	%	0.42 ± 0.04	28.4 ± 2.7	36.8 ± 3.4
Hadrons	n	29525	180	103
	%	98.34 ± 0.07	62.3 ± 2.9	50.5 ± 3.5
Total		30023	289	204

Table 28: Composition of the K^0 samples for various cuts from 1991 Monte Carlo.

		Cuts		
		none	11.*or*.13	13
Mismatch	n	5	0	0
	%	0.03 ± 0.01	0	0
Electrons	n	225	1	0
	%	1.23 ± 0.08	0.06 ± 0.06	0
Prompt μ	n	29	25	24
	%	0.16 ± 0.03	16.2 ± 3.0	25.5 ± 4.5
$Had. \rightarrow \mu$	n	70	37	29
	%	0.38 ± 0.05	24.0 ± 3.4	30.9 ± 4.8
Hadrons	n	18021	91	41
	%	98.21 ± 0.10	59.1 ± 4.0	43.6 ± 5.1
Total		18350	154	94

		Cuts		
		E $\geq$ 91.96	E $\geq$ 91.96 11.*or*.13	E $\geq$ 91.96 13
Mismatch	n	4	0	0
	%	0.04 ± 0.02	0	0
Electrons	n	116	1	0
	%	1.17 ± 0.11	1.6 ± 1.6	0
Prompt μ	n	9	7	7
	%	0.09 ± 0.03	11.1 ± 4.0	18.9 ± 6.4
$Had. \rightarrow \mu$	n	30	14	13
	%	0.30 ± 0.05	22.2 ± 5.2	35.1 ± 7.8
Hadrons	n	9791	41	17
	%	98.40 ± 0.13	65.1 ± 6.0	45.9 ± 8.2
Total		9950	63	37

Table 29: Composition of the K^0 samples for various cuts from 1990 Monte Carlo.

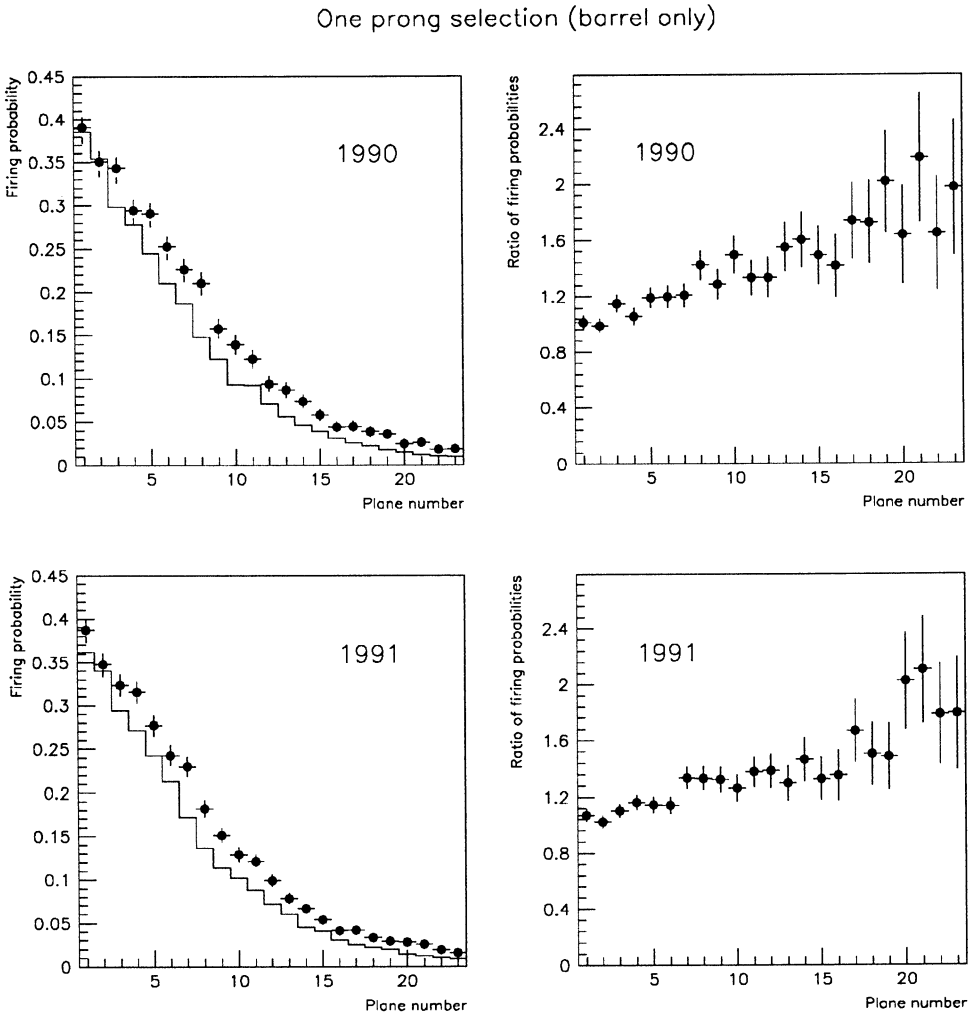

Figure 27: On the left side the probability for a barrel plane to be fired is shown *vs.* the plane number for data (dots) and Monte Carlo (histogram). On the right side the ratio between data and Monte Carlo firing probabilities is shown.

Last - Fired	Data		Monte Carlo	
	n	%	n	%
0	795	41.3 ± 1.1	2942	43.3 ± 0.6
from 1 to 8	1027	53.3 ± 1.1	3617	53.3 ± 0.6
greater than 8	103	5.4 ± 0.5	228	3.34 ± 0.2

Table 30: Last plane - fired planes: comparison from data and Monte Carlo 1991; one–prong sample.

First we will discuss the results obtained with the one–prong selection. 1991 and 1990 will be treated together as there is no significantdifference at the given level of statistical accuracy. In fig. 26 we show the momentum spectra of the selected tracks from data and Monte Carlo, normalized to the same number of tracks. The plots show a good agreement, therefore we will normalize all the forthcoming plots to the number of tracks in the selected momentum bin. Only tracks of momentum greater than 3 GeV/c will be used. For each track we have looked for the hits in the hadron calorimeter laying within the multiple scattering cone of the extrapolated track. The probability for each Barrel plane to be fired by an incoming hadron is shown in fig. 27 where we can see the comparison between the shower development in data and in Monte Carlo. The ratio between data and Monte Carlo is also shown. A clear abundance of "fired planes" is found in data. This is in agreement with what was already known (see [5], [14], [15]) and has not sensibly changed with GEANT version 3.15.

In fig. 28 are shown the distributions of the last fired plane for data and Monte Carlo. (*Last plane* = 0 means that the particle left no signal in the hadron calorimeter).

Up to now, no muon identification cuts have been applied. The identification, in fact, doesn't rely only on penetration criteria, but also uses other characteristics of the shower. In order to clarify to which extent this difference affects the pion misidentification we have studied the standard variables used in muon identification. Before doing that, it is interesting to look at the difference between the number of the last fired plane and the number of fired planes, to see how many times it occurs that a track with a *far* last plane has few fired planes (these tracks are easily rejected).

Last - Fired	Data		Monte Carlo	
	n	%	n	%
0	469	41.1 ± 1.5	2987	42.2 ± 0.6
from 1 to 8	602	52.8 ± 1.5	3791	53.6 ± 0.6
greater than 8	70	6.1 ± 0.7	294	4.2 ± 0.2

Table 31: Last plane - fired planes: comparison from data and Monte Carlo 1990; one–prong sample.

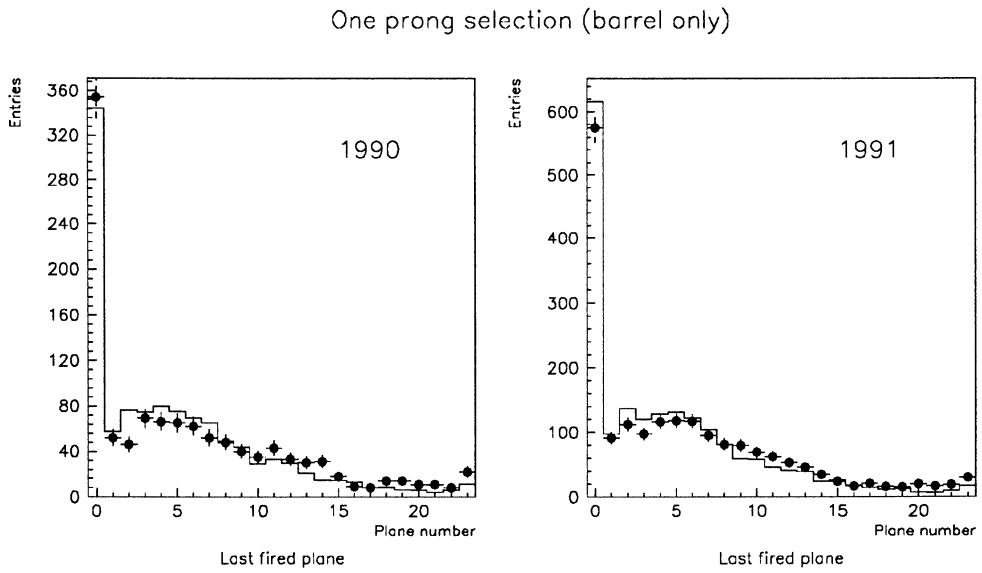

Figure 28: Last fired plane distributions in data (dots) and Monte Carlo (histogram).

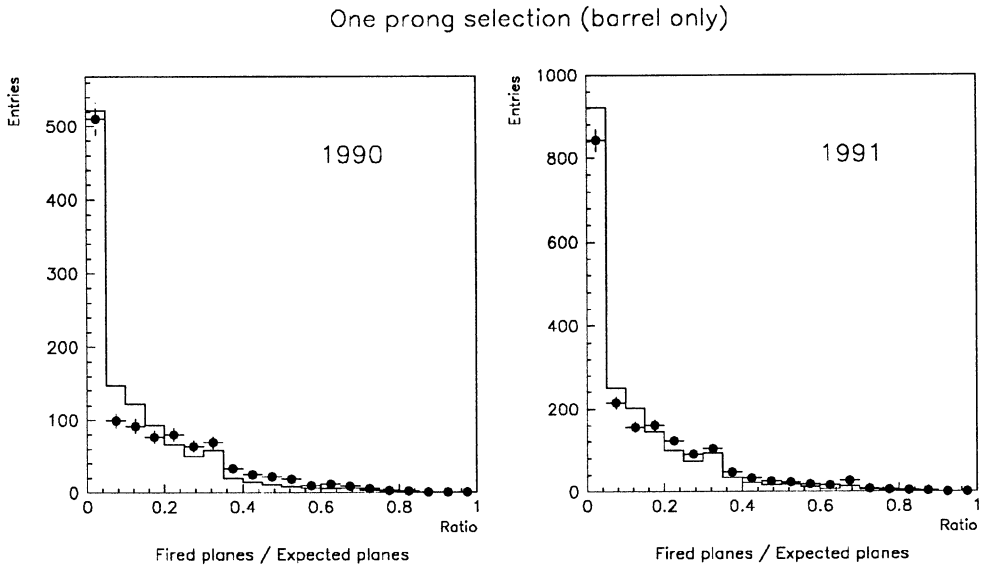

Figure 29: N_{fir}/N_{exp} distributions in data (dots) and Monte Carlo (histogram).

The results, shown in tables 30 and 31, clearly suggest that with a cut based on a larger section of the shower (and not only on the last plane) the difference between data and Monte Carlo should reduce. (In particular we have in mind the cut on the number of fired planes in the last 10 expected).

In fig. 29 we show the distributions of N_{fir}/N_{exp}, where N_{fir} is the number of planes fired and N_{exp} is the number of planes expected to fire according to HCAL geometry and efficiency.

In fig. 30 N_{10} (number of planes fired in last 10 expected) is shown. Requiring the standard muon identification cuts on these variables, *i.e.* $N_{10} \geq 5$ and $N_{fir}/N_{exp} > 0.4$, we get the figures shown in table 32 and 33.

It comes out that requiring the shower to be more *continuous* lowers the difference between data and Monte Carlo. Let's now see what can be found by investigating the transversal shape of the shower.

Another variable used to discriminate hadrons from muons is X_{mult}, the average hits multiplicity in the last ten planes (computed only considering the fired planes, so that it is 0 if there is no hit in the last ten planes, greater or equal to 1 if there are some). Clearly, due to the different average depth of the shower found in data and Monte Carlo, the fraction of tracks for which

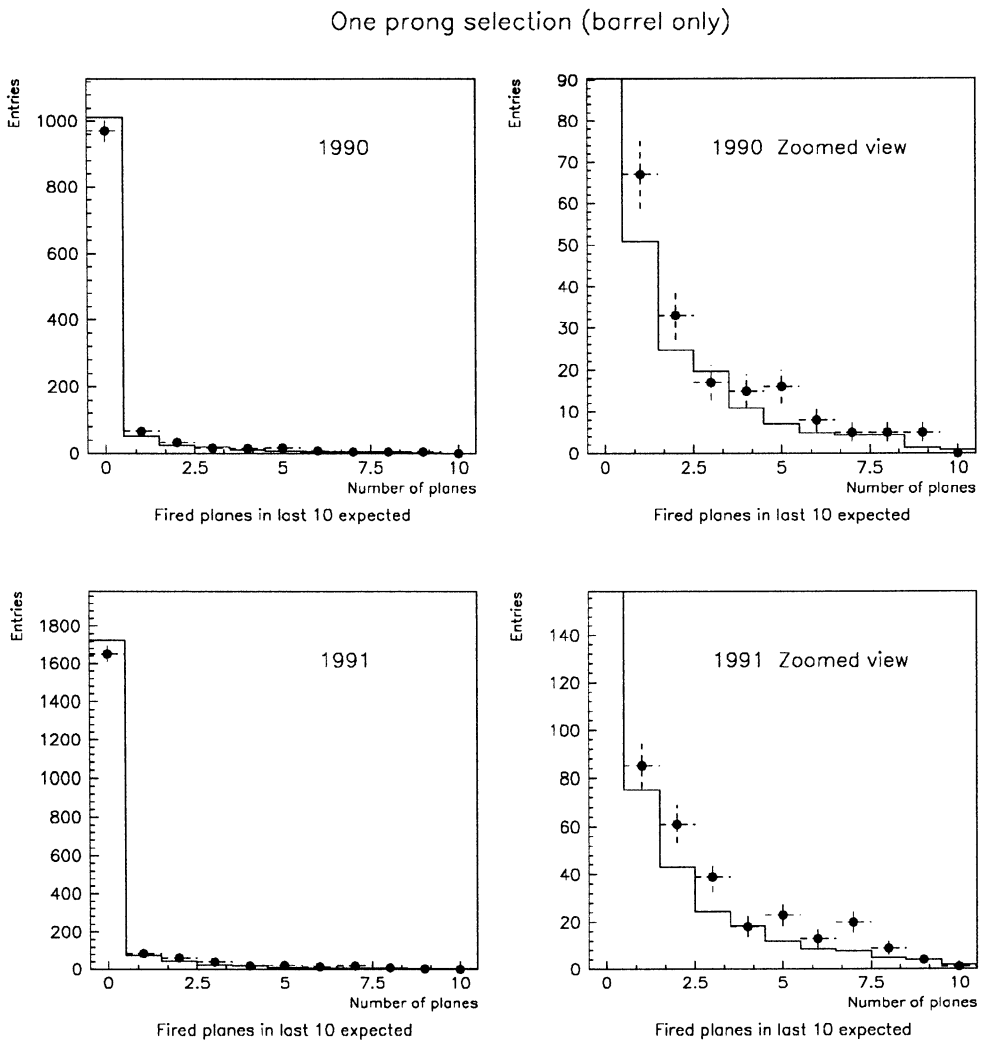

Figure 30: Number of fired planes in the last 10 planes expected to fire in data (dots) and Monte Carlo (histogram).

		$N_{10} \geq 5$	$N_{fir}/N_{exp} > 0.4$
Data	n	71	185
	%	3.69 ± 0.43	9.61 ± 0.67
Monte Carlo	n	143	422
	%	2.11 ± 0.17	6.22 ± 0.29
Ratio		1.75 ± 0.25	1.55 ± 0.13

Table 32: N_{fir}/N_{exp} and N_{10} cuts: comparison from data and Monte Carlo 1991; one–prong sample.

		$N_{10} \geq 5$	$N_{fir}/N_{exp} > 0.4$
Data	n	39	117
	%	3.42 ± 0.54	10.25 ± 0.90
Monte Carlo	n	145	433
	%	2.05 ± 0.17	6.12 ± 0.29
Ratio		1.67 ± 0.30	1.67 ± 0.17

Table 33: N_{fir}/N_{exp} and N_{10} cuts: comparison from data and Monte Carlo 1990; one–prong sample.

	$< X_{mult} >$	
	1991	1990
Data	1.57 ± 0.04	1.58 ± 0.05
Monte Carlo	1.57 ± 0.02	1.62 ± 0.02

Table 34: X_{mult} mean: comparison from data and Monte Carlo for both years.

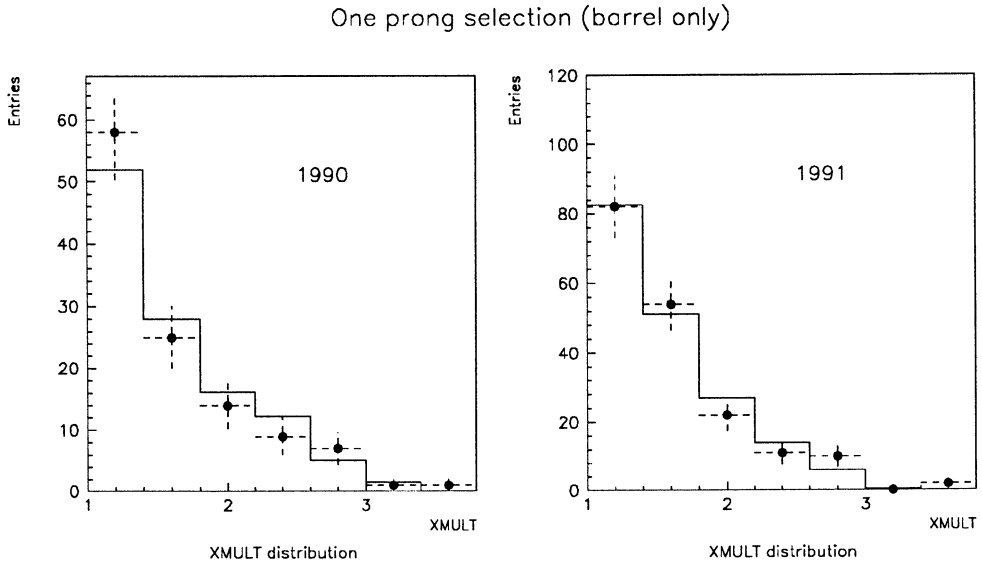

Figure 31: Comparison between X_{mult} distributions in data (dots) and Monte Carlo (histogram). One–prong selection.

the X_{mult} information is available (*i.e.* $X_{mult} \neq 0$) is different. However we are interested in investigating the shape of the X_{mult} distribution for penetrating tracks, so we normalize to the number of tracks having $X_{mult} > 0$, obtaining the plot of fig. 31, which shows a reasonable agreement, while in previous analyses (see [14]) a clear discrepancy was found. Looking at the means of the distributions, we get the values of table 34.

We are now looking at the difference between data and Monte Carlo when we require the full muon identification.

We show in tables 35 and 36 the number of tracks which have QMUIDO flag 11.*or*.13.*or*.14, which includes all the cuts we have mentioned (with $X_{mult} < 1.5$) and a cut on the number of fired planes in the last 3 expected: $N_{03} \geq 1$. or a Muon Chamber hit. In the same tables, in the rows corresponding to QMUIDO flag 13.*or*.14, the hit in the Muon Chamber is always requested. (Flag 14 corresponds to a track which has at least 1 hit in each layer of the muon chambers; it is empty in 1990 when the second layer was not yet implemented). In this case the statistical error is very large and it seems difficult to draw any conclusion as far as differences between data and Monte Carlo are concerned.

		QMUIDO flag	
		11.*or*.13.*or*.14	13.*or*.14
Data	n	24	15
	%	1.25 ± 0.25	0.78 ± 0.20
Monte Carlo	n	61	32
	%	0.90 ± 0.11	0.47 ± 0.08
Ratio		1.39 ± 0.33	1.66 ± 0.51

Table 35: QMUIDO flags: comparison from data and Monte Carlo 1991; one–prong sample.

		QMUIDO flag	
		11.*or*.13	13
Data	n	15	9
	%	1.31 ± 0.34	0.79 ± 0.26
Monte Carlo	n	53	29
	%	0.75 ± 0.10	0.41 ± 0.08
Ratio		1.75 ± 0.51	1.93 ± 0.74

Table 36: QMUIDO flags: comparison from data and Monte Carlo 1990; one–prong sample.

Year	QMUIDO flag	$Had. \rightarrow \mu$	*Hadrons*	$\tau \rightarrow \mu$
1991	11.*or*.13.*or*.14	16	45	0
	13.*or*.14	16	16	0
1990	11.*or*.13	15	37	1
	13	12	16	1

Table 37: Monte Carlo samples composition after μ identification for both years; one–prong selection.

In both years an increase of the ratio between data and Monte Carlo is observed when we ask a muon chamber hit. On one hand this could be due to the fact that this is a *penetration* cut, and, as we have seen, the shower is more penetrating in data. On the other hand the muon chamber hit has two coordinates (while an HCAL hit only one), so its association to the track carries a more detailed information; for this reason we could expect — since we have found that the shower in data is more spread — that the requirement of a muon chamber hit would reduce the misidentification rate in data more than in Monte Carlo. We can't say, at present, whether the observed enhancement of the ratio data/MC is a statistical or a physical effect.

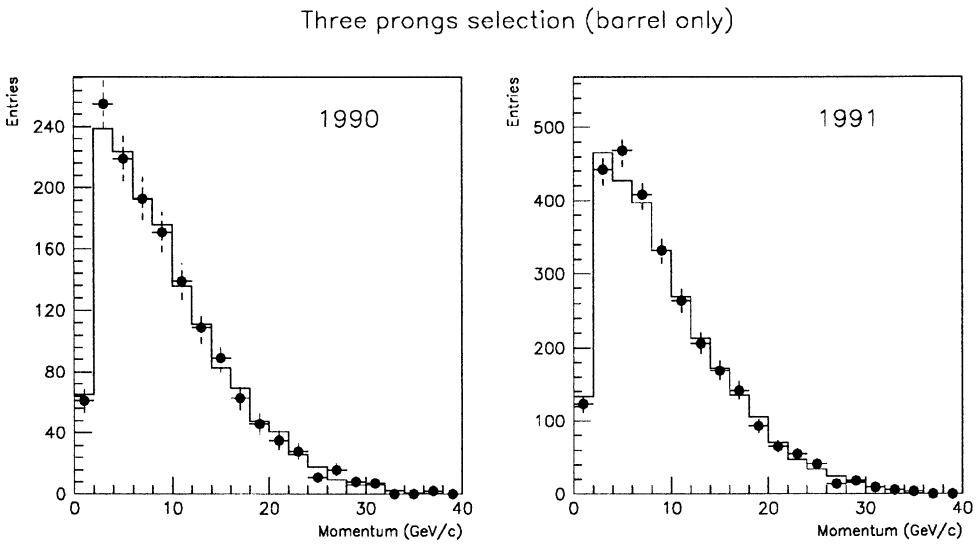

Figure 32: Momentum spectra of the selected tracks in data (dots) and Monte Carlo (histogram).

It's interesting to see the composition of the Monte Carlo sample which is left after muon identification cuts. In table 37 the number of selected tracks is quoted for both 1991 and 1990 Monte Carlo: it is clear that a very high initial hadron purity is required to have a reasonable pure sample also after μ identification.

The two samples of Monte Carlo have been carefully checked using the information on the *true* tracks, and we verified that the interaction cross

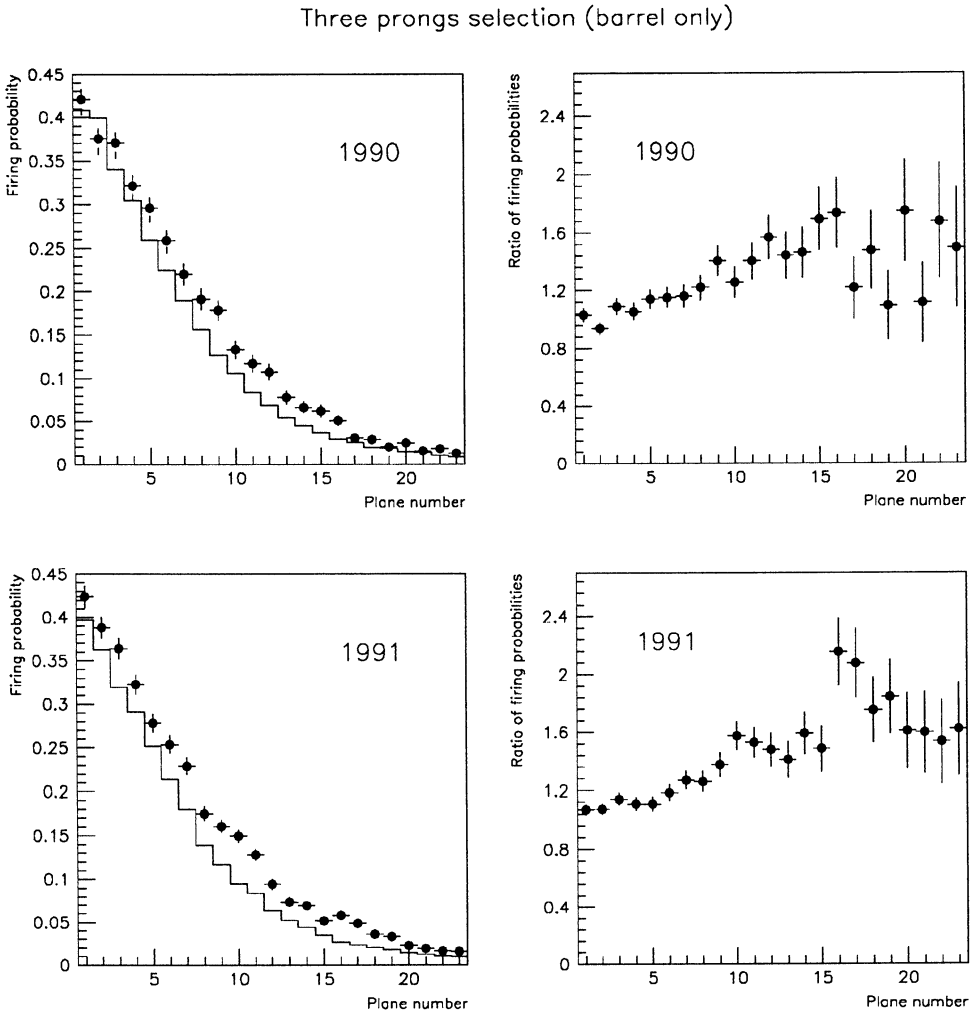

Figure 33: On the left side the probability for a barrel plane to be fired is shown *vs.* the plane number for data (dots) and Monte Carlo (histogram). On the right side the ratio between data and Monte Carlo firing probabilities is shown.

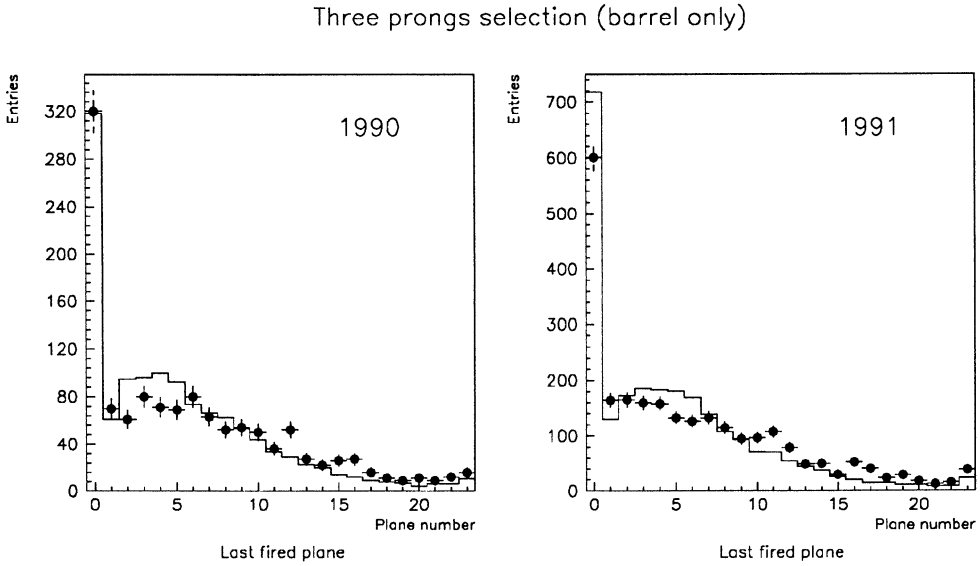

Figure 34: Last fired plane distributions in data (dots) and Monte Carlo (histogram).

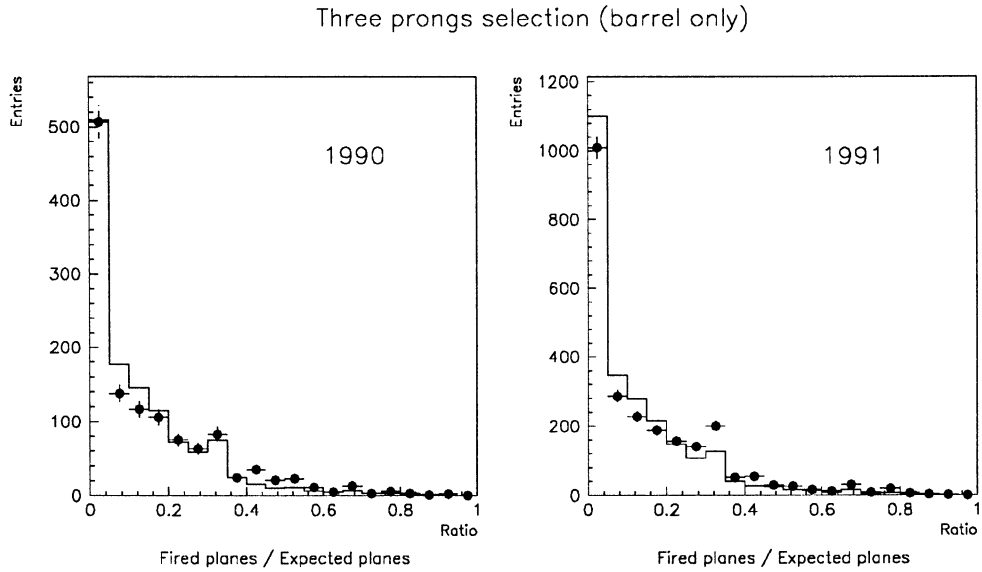

Figure 35: N_{fir}/N_{exp} distributions in data (dots) and Monte Carlo (histogram).

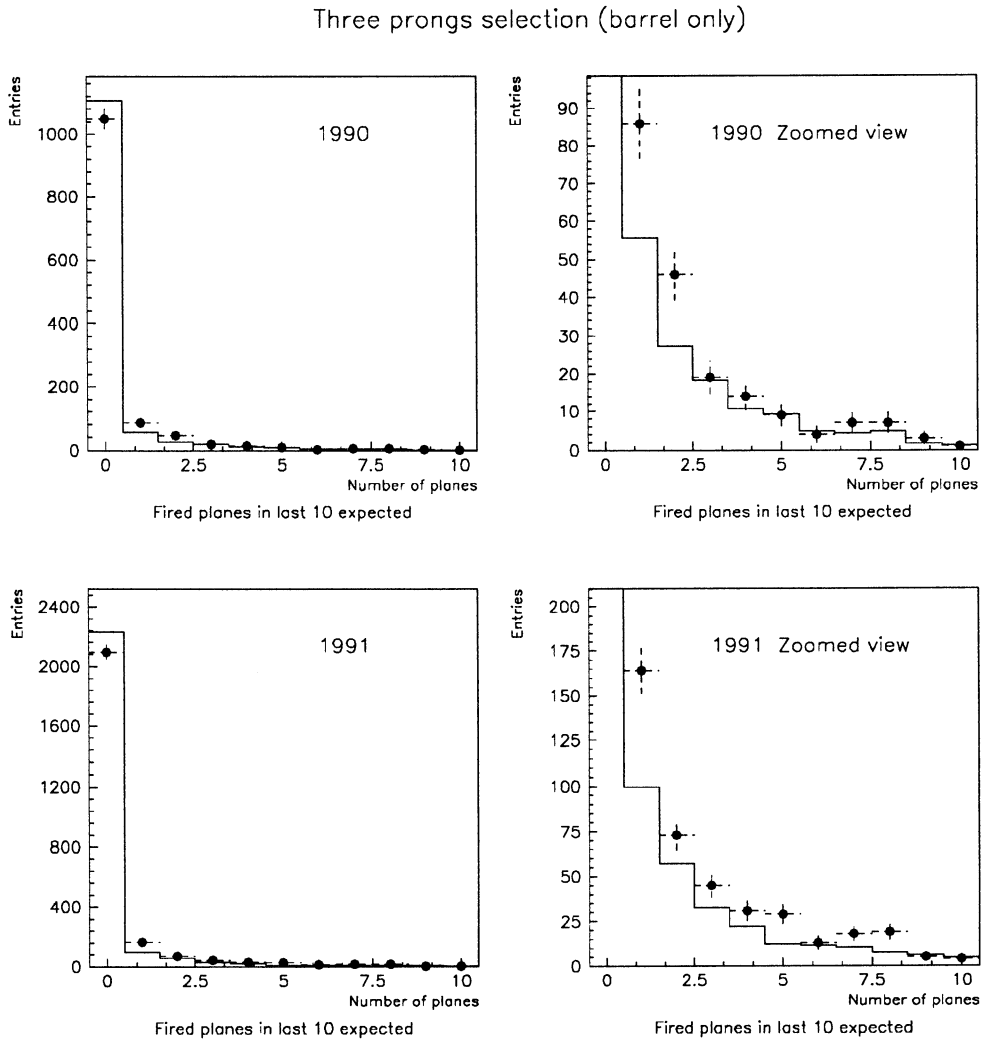

Figure 36: Number of fired planes in the last 10 planes expected to fire in data (dots) and Monte Carlo (histogram).

Last - Fired	Data		Monte Carlo	
	n	%	n	%
0	977	39.1 ± 1.0	3486	41.9 ± 0.5
from 1 to 8	1345	53.9 ± 1.0	4542	54.7 ± 0.5
greater than 8	175	7.0 ± 0.5	281	3.4 ± 0.2

Table 38: Last plane - fired planes: comparison from data and Monte Carlo 1991; three–prong sample.

Last - Fired	Data		Monte Carlo	
	n	%	n	%
0	482	38.7 ± 1.4	3441	38.9 ± 0.5
from 1 to 8	670	53.9 ± 1.4	5051	57.2 ± 0.5
greater than 8	92	7.4 ± 0.7	346	3.9 ± 0.2

Table 39: Last plane - fired planes: comparison from data and Monte Carlo 1990; three–prong sample.

section is the same. Nevertheless the the results of the two years cannot be averaged when we are using also muon chamber hits, as in 1991 there is one more layer.

These results are valid for pions with a momentum spectrum typical of single–prong τ decays. At present we don't have enough statistics to be able to give results in function of the track momentum.

We have repeated the same analysis on the three–prong sample. The main differences between this sample and the previous one, are a greater amount of decays (due to the softer spectrum) and the fact that now we have three shower superimposed, instead of one isolated particle, since the three π from the τ decay are very collimated. This results in quite different features, which are shown in figg. 32–36 and tables 38–43.

In particular the shower developments are very similar to the one–prong ones in the first part of the calorimeter, while we find much less disagreement in the last part (where decays are dominating).

		$N_{10} \geq 5$	$N_{fir}/N_{exp} > 0.4$
Data	n	90	235
	%	3.60 ± 0.37	9.41 ± 0.58
Monte Carlo	n	176	533
	%	2.12 ± 0.16	6.41 ± 0.27
Ratio		1.70 ± 0.22	1.47 ± 0.11

Table 40: N_{fir}/N_{exp} and N_{10} cuts: comparison from data and Monte Carlo 1991; three–prong sample.

		$N_{10} \geq 5$	$N_{fir}/N_{exp} > 0.4$
Data	n	31	131
	%	2.49 ± 0.44	10.53 ± 0.87
Monte Carlo	n	193	560
	%	2.18 ± 0.16	6.34 ± 0.26
Ratio		1.14 ± 0.22	1.66 ± 0.15

Table 41: N_{fir}/N_{exp} and N_{10} cuts: comparison from data and Monte Carlo 1990; three–prong sample.

		QMUIDO flag	
		11.*or*.13.*or*.14	13.*or*.14
Data	n	24	19
	%	0.96 ± 0.20	0.76 ± 0.17
Monte Carlo	n	73	51
	%	0.88 ± 0.10	0.61 ± 0.09
Ratio		1.09 ± 0.26	1.25 ± 0.33

Table 42: QMUIDO flags: comparison from data and Monte Carlo 1991; three–prong sample.

		QMUIDO flag	
		11.*or*.13	13
Data	n	11	5
	%	0.88 ± 0.27	0.40 ± 0.18
Monte Carlo	n	72	41
	%	0.81 ± 0.10	0.46 ± 0.07
Ratio		1.09 ± 0.36	0.87 ± 0.41

Table 43: QMUIDO flags: comparison from data and Monte Carlo 1990; three–prong sample.

Year	QMUIDO flag	$Had. \rightarrow \mu$	*Hadrons*
1991	11.*or*.13.*or*.14	26	47
	13.*or*.14	22	29
1990	11.*or*.13	26	46
	13	24	17

Table 44: Monte Carlo samples composition after μ identification for both years; three–prong selection.

Last - Fired	Data		Monte Carlo	
	n	%	n	%
0	5919	47.73 ± 0.45	14709	48.99 ± 0.29
from 1 to 8	5828	46.99 ± 0.45	14055	44.82 ± 0.29
greater than 8	655	5.28 ± 0.20	1259	4.19 ± 0.12

Table 45: Last plane - fired planes: comparison from data and Monte Carlo 1991; K^0 sample.

Last - Fired	Data		Monte Carlo	
	n	%	n	%
0	3114	48.54 ± 0.62	4776	48.00 ± 0.50
from 1 to 8	2920	45.52 ± 0.62	4886	49.11 ± 0.50
greater than 8	381	5.94 ± 0.30	288	2.89 ± 0.17

Table 46: Last plane - fired planes: comparison from data and Monte Carlo 1990; K^0 sample.

The numbers given in the tables show similar features to the ones quoted for the one–prong selection, but with a lower disagreement. In the case of 1990 we find even less efficiency in data than in Monte Carlo when require one hit in the muon chambers.

In table 44 Monte Carlo compositions are shown for the samples obtained with full μ identification. In this case the decay fractions in the final samples are larger than in the one–prong samples.

In figg. 37–41 and tables 45–50 we give the results for the K^0 selection. The composition of this sample is very similar to the three–prong one, the only difference being a higher amount of decaying with respect to non–decaying hadrons (due to the softer spectrum) and the presence of some *prompt* muons in the selection. The features of these samples are completely consistent with the three–prong ones, the only clear difference being higher statistics and therefore less fluctuations.

The Monte Carlo compositions have been already shown in the event

		$N_{10} \geq 5$	$N_{fir}/N_{exp} > 0.4$
Data	n	337	974
	%	2.72 ± 0.15	7.85 ± 0.24
Monte Carlo	n	723	892
	%	2.41 ± 0.09	5.73 ± 0.13
Ratio		1.13 ± 0.08	1.37 ± 0.05

Table 47: N_{fir}/N_{exp} and N_{10} cuts: comparison from data and Monte Carlo 1991; K^0 sample.

		$N_{10} \geq 5$	$N_{fir}/N_{exp} > 0.4$
Data	n	145	477
	%	2.26 ± 0.19	7.44 ± 0.33
Monte Carlo	n	179	580
	%	1.80 ± 0.13	5.83 ± 0.23
Ratio		1.26 ± 0.14	1.28 ± 0.08

Table 48: N_{fir}/N_{exp} and N_{10} cuts: comparison from data and Monte Carlo 1990; K^0 sample.

		QMUIDO flag	
		11.*or*.13.*or*.14	13.*or*.14
Data	n	125	81
	%	1.01 ± 0.09	0.65 ± 0.07
Monte Carlo	n	289	204
	%	0.96 ± 0.06	0.68 ± 0.05
Ratio		1.05 ± 0.10	0.96 ± 0.15

Table 49: QMUIDO flags: comparison from data and Monte Carlo 1991; K^0 sample.

		QMUIDO flag	
		11.*or*.13	13
Data	n	59	32
	%	0.92 ± 0.12	0.50 ± 0.09
Monte Carlo	n	63	37
	%	0.63 ± 0.08	0.37 ± 0.06
Ratio		1.46 ± 0.27	1.35 ± 0.33

Table 50: QMUIDO flags: comparison from data and Monte Carlo 1990; K^0 sample.

selection subsection, before and after μ identification.

A.3 Conclusions

Now we will try to extract from the collected numbers, a correction factor to apply for *punch-throughs*, which are clearly not well simulated. We are dealing now only with the final μ identification cut (QMUIDO flag 13.*or*.14 in 1991, QMUIDO flag 13 in 1990) which is used in most analyses, all the other part of this study being devoted to convince ourselves that we are not seeing statistical fluctuations, and to investigate the features and the sources of the discrepancies.

Summarizing what we have understood about the matter, we can say that there are certainly some discrepancies between data and simulation as far as hadronic showers are concerned, and these discrepancies are not only related to the depth of the showers, but involve other features. So we cannot draw any conclusion studying the number of hadrons which reach the last part of the calorimeter, but we really have to study the effects of the identification cuts in data and Monte Carlo. This obviously leads to a dramatic decrease of the statistics, which is the main problem of this study.

Moreover, it seems that the discrepancy is not exactly the same when we consider isolated showers or collimated hadrons, and so it should be again different for the hadrons which contaminate our muon sample in the analysis, since they are rather isolated (we apply a $p_\perp$ cut), but still inside a jet in a hadronic event.

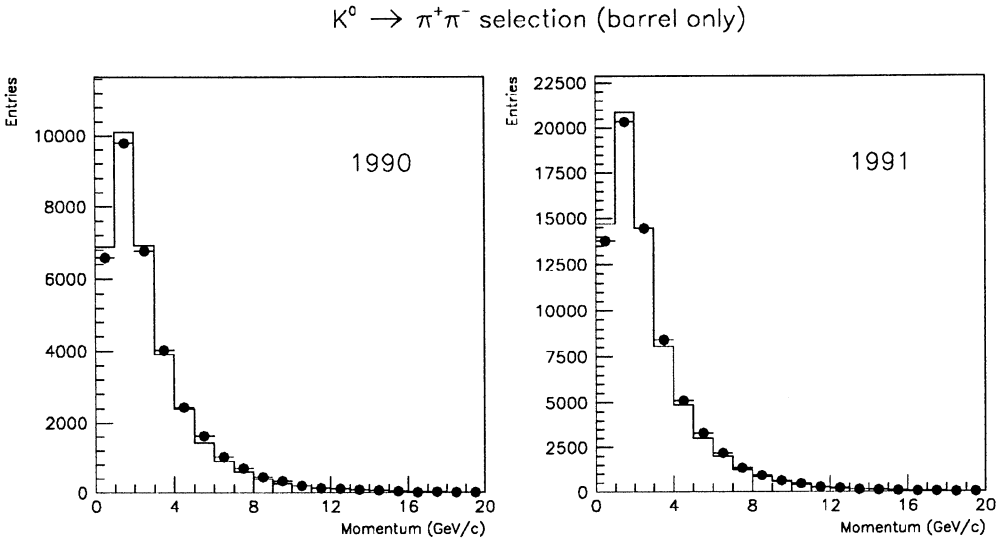

Figure 37: Momentum spectra of the selected tracks in data (dots) and Monte Carlo (histogram).

On the contrary, there seems to be no significant differences between the two Monte Carlo samples (which use different versions of GEANT), and this has been carefully checked comparing two samples of single pions, generated with the two versions.

The aim of this study was to get a correction factor to apply to the background amount predicted by the Monte Carlo. Given the small statistics available, we see no other way than merging the information from the three samples of both years, even if this is not completely correct, as we have discussed previously. In doing that we keep the decay correction factor frozen to 1, since the decay simulation relies basically on the lifetime and semileptonic branching ratio of pions, which are well known. (This is true because we have defined *decays* only the decays in the TPC volume, while decays in the calorimeter are included in the *hadron* class). Taking into account the sample composition after muon identification cuts, we get the ratio of misidentification probability in data and Monte Carlo:

$$R_{punch-through} = 1.16 \pm 0.22 \pm 0.05$$

where the first error is statistic and the second comes from the uncertainty in the sample composition.

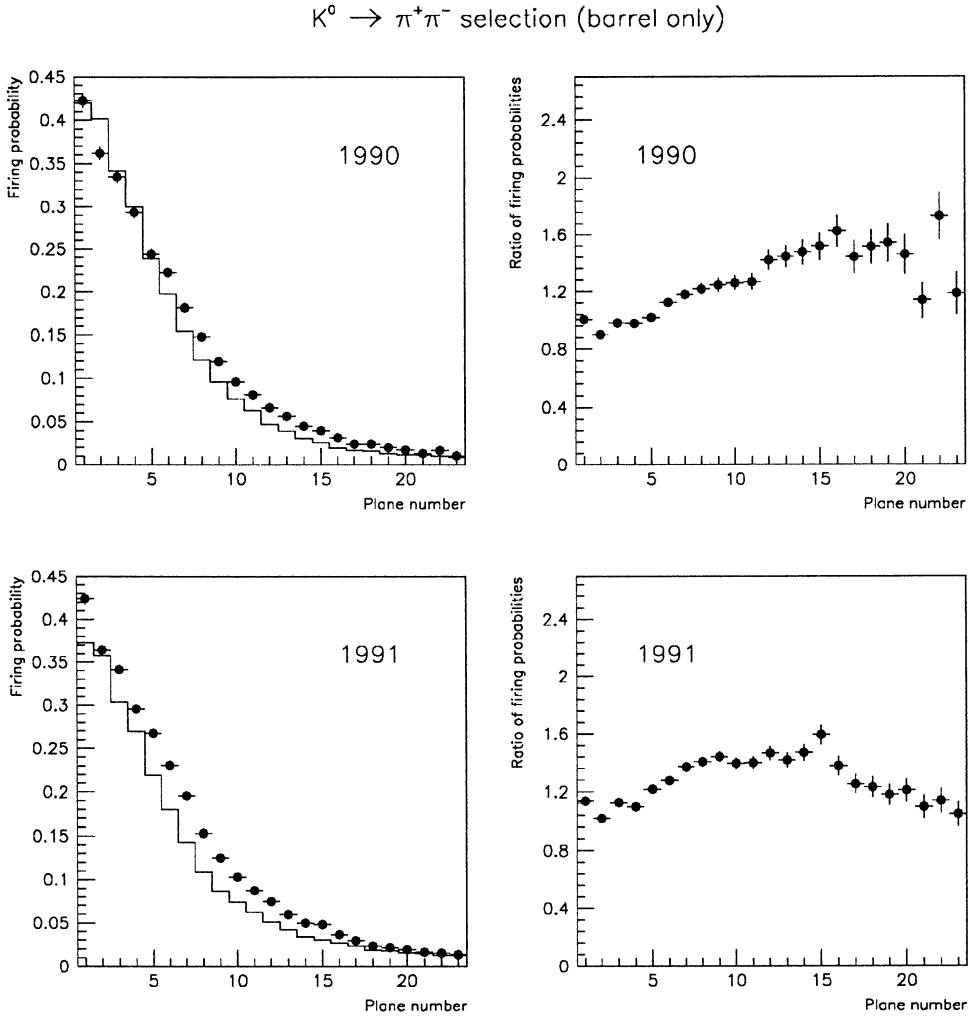

Figure 38: On the left side the probability for a barrel plane to be fired is shown *vs.* the plane number for data (dots) and Monte Carlo (histogram). On the right side the ratio between data and Monte Carlo firing probabilities is shown.

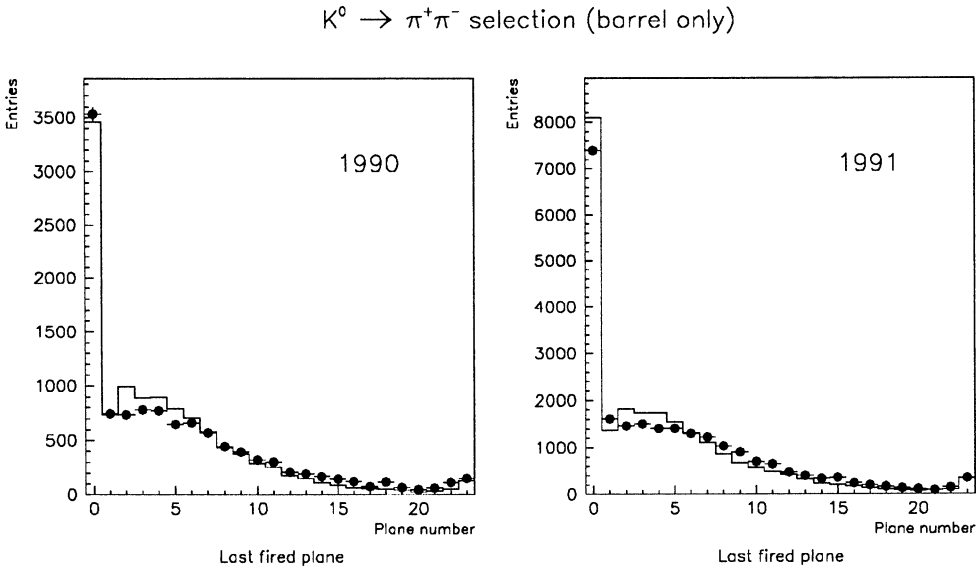

Figure 39: Last fired plane distributions in data (dots) and Monte Carlo (histogram).

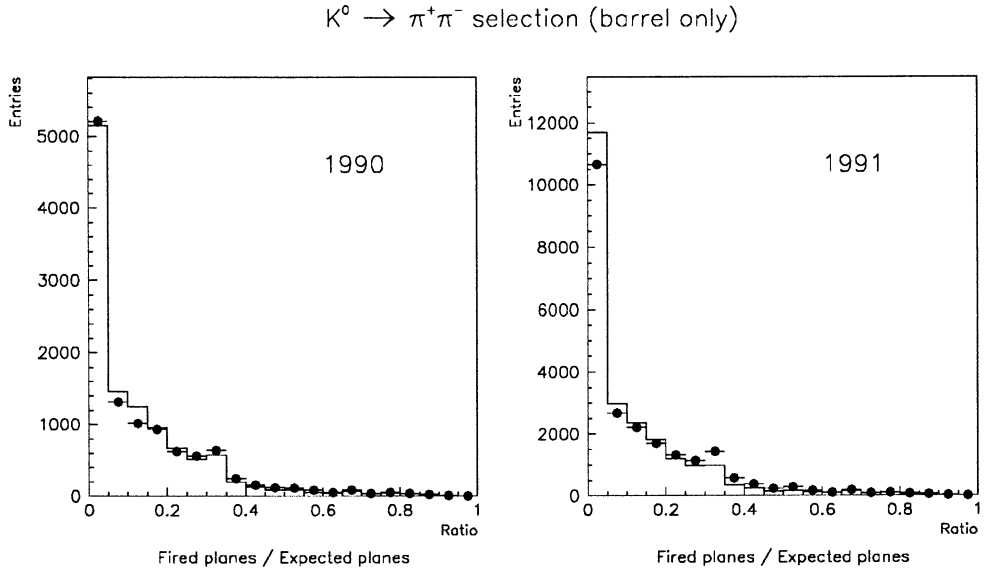

Figure 40: N_{fir}/N_{exp} distributions in data (dots) and Monte Carlo (histogram).

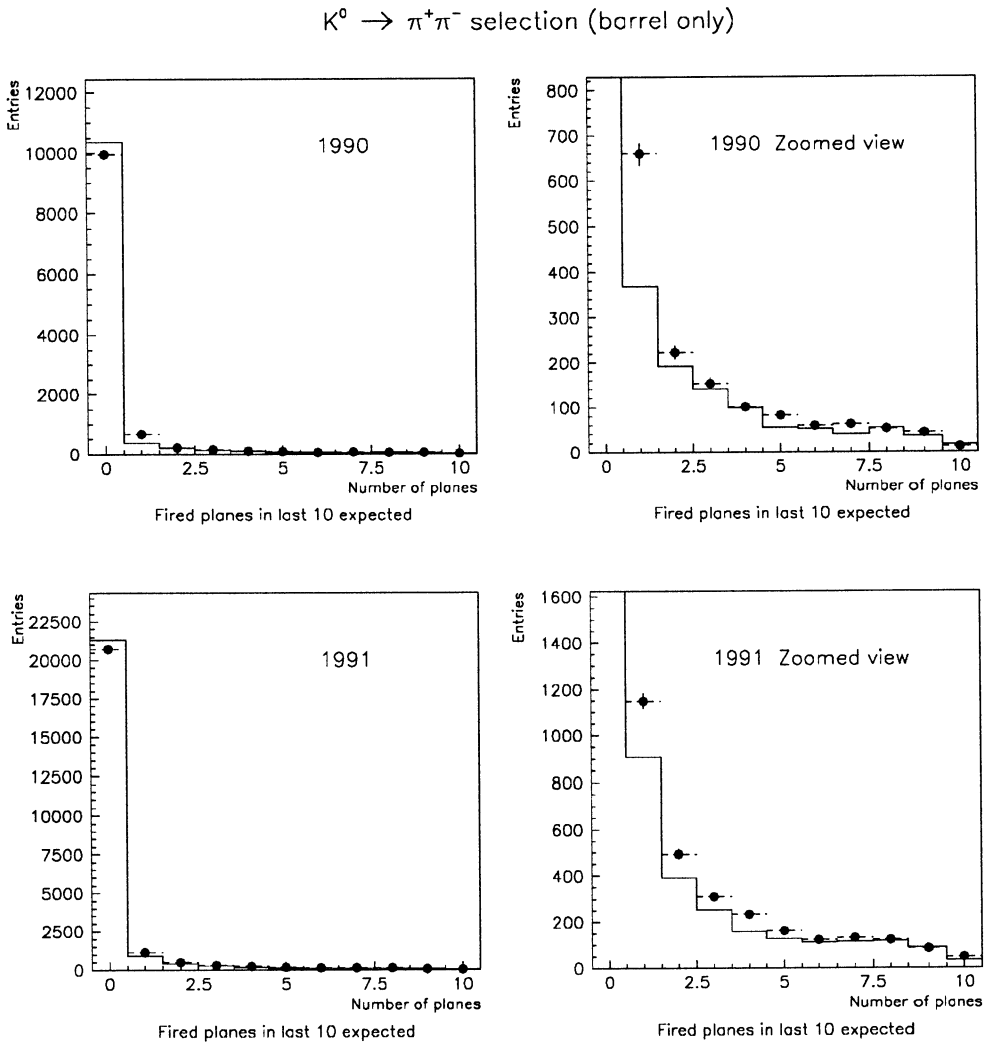

Figure 41: Number of fired planes in the last 10 planes expected to fire in data (dots) and Monte Carlo (histogram).